ANNUAL REVIEWS

Annual Review of Materials Research

Strain Glass State, Strain Glass Transition, and Controlled Strain Release

Dong Wang,[1] Yuanchao Ji,[1] Xiaobing Ren,[2] and Yunzhi Wang[3]

[1]Center of Microstructure Science, Frontier Institute of Science and Technology, State Key Laboratory for Mechanical Behavior of Materials, Xi'an Jiaotong University, Xi'an, China; email: wang_dong1223@xjtu.edu.cn, jyc.xjtu@xjtu.edu.cn

[2]Research Center for Functional Materials, National Institute for Materials Science, Tsukuba, Ibaraki, Japan; email: REN.Xiaobing@nims.go.jp

[3]Department of Materials Science and Engineering, College of Engineering, The Ohio State University, Columbus, Ohio, USA; email: wang.363@osu.edu

Annu. Rev. Mater. Res. 2022. 52:159–87

First published as a Review in Advance on April 8, 2022

The *Annual Review of Materials Research* is online at matsci.annualreviews.org

https://doi.org/10.1146/annurev-matsci-081720-091919

Keywords

structural transformation, martensite, nanodomains, linear superelasticity, shape memory alloys

Abstract

Strain glass is a new strain state discovered recently in ferroelastic systems that is characterized by nanoscale martensitic domains formed through a freezing transition. These nanodomains typically have mottled or tweed morphology depending on the elastic anisotropy of the system. Strain glass transition is a broadly smeared and high order–like transition, taking place within a wide temperature or stress range. It is accompanied by many unique properties, including linear superelasticity with high strength, low modulus, Invar and Elinvar anomalies, and large magnetostriction. In this review, we first discuss experimental characterization and testing that have led to the discovery of the strain glass transition and its unique properties. We then introduce theoretical models and computer simulations that have shed light on the origin and mechanisms underlying the unique characteristics and properties of strain glass transitions. Unresolved issues and challenges in strain glass study are also addressed. Strain glass transition can offer giant elastic strain and ultralow elastic modulus by well-controlled reversible structural phase transformations through defect engineering.

1. INTRODUCTION

Structural phase transformation is a fundamental carrier of both elastic (reversible) and plastic (irreversible) strains and offers many novel physical, mechanical, and functional properties that conventional elasticity and plasticity carriers cannot offer, including giant elastic response [also called pseudo- or superelasticity (SE)] (1, 2), shape memory effect (SME) (3, 4), Invar and Elinvar anomalies (5–7), piezoelectricity (8), and electro- and magnetostrictions (9, 10). However, because structural phase transformations behave so differently from the intrinsic elastic carrier (change in atomic bound length and angle) and conventional plastic carriers (such as dislocations), they may have been overlooked as general elasticity/plasticity carriers and thus underappreciated in alloy design. For example, the strain release by a structural phase transformation is usually highly nonlinear, taking place in an avalanche fashion within a narrow temperature or stress range, and is difficult to control. Therefore, the main objective of the current review is to put together recent experimental and theoretical efforts devoted to regulating and utilizing structural phase transformations for controlled elastic and plastic strain release under applied external fields. Since controlled plastic strain release and enhanced work-hardening capacity by phase transformations in transformation-induced plasticity steels and Ti alloys have been reviewed recently (11–13), the current review focuses on strain glass transition and controlled pseudoelastic strain release.

A typical example of utilizing structural phase transformations as strain carriers in alloy design is the development of shape memory alloys (SMAs) that have attracted much attention because of their SME and SE (14). The SME and SE have led to many advanced applications of SMAs in robotics, automotive, aerospace, and biomedical fields (15–17). However, the structural phase transformation that underpins the SME and SE of SMAs, called martensitic transformation, is sharp, strongly first order, and shear dominant. It propagates at the velocity of sound traveling in solids and produces self-accommodating long-range ordered strain domains by autocatalysis. The individual domains are called martensitic variants (or transformation variants or deformation variants), and the long-range ordered strain domain patterns can be regarded as strain crystals, in contrast to the dynamic strain fluctuations present in austenite (strain liquid) (18) as shown schematically in **Figure 1**. The responses of martensitic transformations to external fields such as stress and temperature are highly nonlinear, showing large stress-strain or temperature-strain hysteresis and narrow stress or temperature range of activation. These characteristics have made them unsuitable for applications requiring high positioning accuracy, wide temperature windows, and low energy loss.

In recent years, extensive efforts have been made both experimentally and theoretically to tame martensitic transformations for controlled strain release. One way of doing so is to turn the sharp, strongly first-order martensitic transformation into a broadly smeared, apparently continuous, high order–like strain glass transition by defect engineering. The strain glass transition was first reported in $Ni_{50+x}Ti_{50-x}$ SMAs by doping with excess Ni ($x \geq 1.5$). It is characterized by the formation of mottled nanodomains of martensite (i.e., a strain glass state) through a freezing transition and exhibits a continuous transformation behavior upon loading/unloading or cooling/heating cycling (18). Strain glass describes a structural state with static (dynamically frozen) nanodomains of transformation strains (i.e., martensitic variants). These nanodomains typically have mottled or tweed morphology depending on the elastic anisotropy of the system, similar to the microstructure seen during a premartensitic transformation where the nanodomains are partially frozen. The transformation strains are the order parameters that characterize structural phase transformations dominated by shear (i.e., shape change of the crystal unit cell). Such a structural state differs from the two known states of martensitic systems: a strain crystal consisting of long-range ordered strain domains such as those internally twinned herringbone martensitic structures and a strain liquid

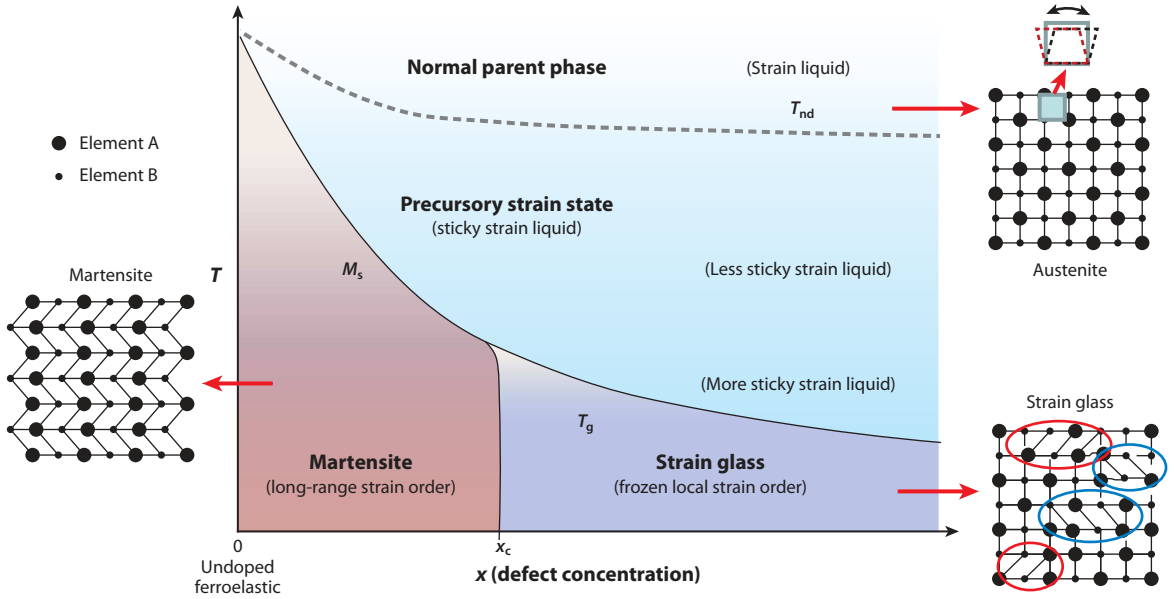

Figure 1

Strain-state (i.e., strain liquid, strain crystal, and strain glass) diagram of ferroelastic systems (19). T_{nd}, M_s, and T_g represent the transition temperature of nanodomain formation, martensitic phase transformation start temperature, and strain glass transition temperature, respectively. The strain state changes from a strain liquid (the parent phase, with weak and random strain fluctuations) to a partially frozen, sticky strain liquid (a precursory strain state, with some static nanodomains of martensite) to a strain crystal (normal martensite, with long-range ordered strain domains that arrange into a self-accommodating polytwin pattern) at low defect concentrations or to a strain class (fully frozen nanodomains of martensite, with the nanodomains represented by *red and blue ovals*) at high defect concentrations. Figure adapted with permission from Reference 19; copyright 2010 Taylor & Francis.

consisting of random and dynamic strain domains that are present in austenite (19). These three strain states and their relationships are shown in the strain-state phase diagram in **Figure 1**.

Strain glass belongs to the family of ferroic glasses, which also includes spin glass/cluster spin glass and relaxor ferroelectrics (ferroelectric glasses) (20, 21). Although spin glass/cluster spin glass and relaxor ferroelectrics were discovered many decades ago, frozen tweed (i.e., strain glass) (22) was first shown by computer simulations in martensitic systems in the 1990s, and strain glass transition was first discovered by experimental measurements in 2005 (18). These ferroic glasses are defined by disordered states or nanodomains of their corresponding order parameters that characterize the ferroic phase transformations [i.e., strain in strain glass, spin in spin glass, and polarization in relaxor (**Figure 2*a***)], which is different from oxide glasses or metallic glasses that have disordered atomic structures. In other words, oxide and metallic glasses are amorphous, while ferroic glasses are crystalline. The ferroic glass states are characterized by nanodomains of the order parameters (spin, electric dipole, and lattice strain) (**Figure 2*b***) and frequency dispersion of elastic stiffness S [the inverse of elastic modulus (i.e., E^{-1})], dielectric permittivity ε, and magnetic susceptibility χ' (**Figure 2*c***).

Stress-carrying defects such as point defects, nanoprecipitates, and dislocations will create local lattice distortions and generate a random stress/strain field that interferes with the nucleation and growth of martensite. If such a random stress/strain field percolates in the system (23, 24), it will completely suppress autocatalytic events during nucleation and growth and prevent the formation of self-accommodating long-range ordered transformation strain patterns (e.g., internally

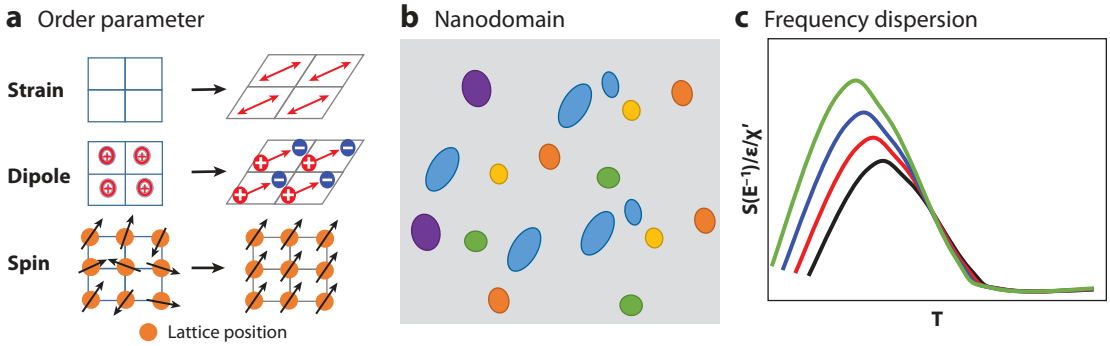

Figure 2

The parallelism among the three ferroic glasses. (*a*) Order parameters (strain, electric dipole, and spin) characterizing the ferroic states. The strain describes the shear from a high symmetry phase (cubic lattice) to a low symmetry phase (parallelogram lattice) with the double-sided arrows representing the strain tensor. The electric dipole describes the charge displacement due to the symmetry change, with red arrows representing the electric dipole vectors. The spin ordering describes the change of magnetic interaction, with black arrows representing the spin vectors at different lattice positions. (*b*) Nanodomain structures of ferroic glasses. Different colored ovals represent nanodomains with different variants (i.e., different arrow directions). (*c*) Frequency dispersion of stiffness S (the inverse of elastic modulus E^{-1}), dielectric permittivity ε, and magnetic susceptibility χ' for strain glass, relaxor, and spin glass, respectively. Different colored lines represent different frequencies.

twinned herringbone structures in martensite) and, thus, render a sharp martensitic transformation a smooth strain glass transition (18, 25–30). A strain glass transition is smooth because the local stress field from random defects induces the formation of certain martensitic variants at temperatures much higher than the martensitic transformation start temperature, M_s, or at stress levels much lower than the critical stress for stress-induced martensitic transformation, σ_0, of the defect-free counterpart. The growth of these martensitic domains is confined by the adjacent non-self-accommodating domains (because they are induced by the random defects, not by autocatalysis), and, thus, the transformation goes to completion at a much lower temperature or much higher stress.

Figure 1 shows a strain-state transition diagram (or phase diagram for short) in ferroelastic systems. At relatively high temperatures, the high symmetry parent phase (i.e., austenite) is stable, but strain fluctuations at nanometer scale occur dynamically in the system, and the amplitudes of the fluctuations depend on the curvature of the Landau free energy at zero strain at a given temperature. This is the strain liquid state. The martensitic phase becomes more and more stable as the temperature decreases, and the system will transform into either a long-range ordered strain domain pattern such as that seen in internally twinned herringbone martensite if the defect concentration is below a critical value or a nanodomain pattern of martensite having mottled or tweed morphology, depending on the elastic anisotropy of the system, if the defect concentration exceeds a critical value. The former is a strain crystal, while the latter is a strain glass.

Compared to a normal martensitic transformation, strain glass transition exhibits many unusual characteristics, including nearly linear SE with almost zero hysteresis upon cooling and heating (that underpins the Invar and Elinvar anomalies) and with ultralow elastic modulus upon loading and unloading, the disappearance of thermal peaks in differential scanning calorimetry (DSC), invariance of average structure from X-ray diffraction (XRD), and frequency dispersion of storage modulus from dynamic mechanical analysis (DMA) (18, 25). As a glass state, strain glass and the other ferroic glasses (cluster spin glass and relaxor in ferromagnetic and ferroelectric systems, respectively) have shown similar or parallel characteristics as conventional oxide and metallic glasses:

disorder state of the order parameters that characterize the ferroic states (i.e., strain, polarization, and magnetization), frequency dispersion or relaxation, continuous freezing process, and crystallization during long-term aging (31, 32). However, ferroic glasses also exhibit some unusual kinetic characteristics compared to oxide and metallic glasses. For example, the strain glass transition becomes faster at lower temperatures (i.e., colder is faster) (33), which is in sharp contrast to the so-called colder-is-slower transition behavior of oxide and metallic glasses. Such a difference can be attributed to the competition between activation entropy and activation enthalpy, which unveils the change from colder is faster to colder is slower with the increase of defect concentration (33).

Since their discovery in 2005, many strain glass systems have been reported, including point defect–doped TiNi (25, 26, 34, 35), TiNb (6), TiPd (36–38), TiAu (39), FeMnGa (40), NiCoGa (41), and NiMnIn (42), as well as SMAs with densely populated nanoscale precipitates (27, 28) or that are heavily cold worked (29, 30). According to the characteristics of a strain glass state and a strain glass transition mentioned above, a strain glass system can be identified by the following four pieces of experimental evidence to show (*a*) the existence of nano-sized martensitic domains by transmission electron microscopy (TEM) observations, (*b*) frequency dispersion of the storage modulus following Vogel-Fulcher relation from DMA, (*c*) invariance of average structure from XRD or disappearance of phase transition peak from DSC, and (*d*) continuous loss of ergodicity upon cooling from mechanical zero-field cooling/field cooling testing (**Figure 3**).

Below, we first discuss experimental characterizations of strain glass systems in Section 2, followed by theoretical analysis and computer simulations of strain glass transition in Section 3. We then present some challenges and outlooks of strain glass study in Section 4, followed by concluding remarks in Section 5.

2. EXPERIMENTAL CHARACTERIZATION AND TESTING OF STRAIN GLASS STATE AND STRAIN GLASS TRANSITION

Relaxor ferroelectrics were discovered in the 1960s, and cluster spin glass was discovered in 1972 (21), all by point defect doping. However, it was not until 2005, when the first strain glass system was reported in $Ti_{50-x}Ni_{50+x}$ with doping of excess amounts of antisite defect of Ni ($x = 1.5$) (18), that the spectrum of ferroic glasses was completed (21). Since its discovery, strain glass has been reported in different ferroelastic systems by point defect doping (5, 6, 25, 26, 34–36, 38, 41, 43–46).

Sufficient point defect doping is necessary for the formation of strain glasses with relatively small transformation strains. As the point defect concentration increases, the martensitic domain size decreases, and when the point defect concentration exceeds a critical value, the microstructure of the system changes from a long-range ordered, internally twinned domain structure consisting of self-accommodating martensitic variants into mottled or tweed nanodomains of martensite (i.e., a strain glass state) depending on the elastic anisotropy of the system. **Figure 3*a*,*e*** shows the typical microstructures of strain crystal (normal martensite) and strain glass states where the difference between the degrees of strain order becomes evident. In TiNi-X SMAs, the strain glass transition requires different critical concentrations for different types of dopants, which could be attributed to their atomic radius differences and thus different lattice strains generated. The critical concentration of a given type of dopant for strain glass transition also depends on the elastic anisotropy of the system (47, 48).

Since relaxors and spin glasses are created solely by point defect doping, early studies on strain glasses also focused on point defects. However, any stress-carrying defects at high enough densities should be able to serve the same (or even more effective) role as point defects in strain

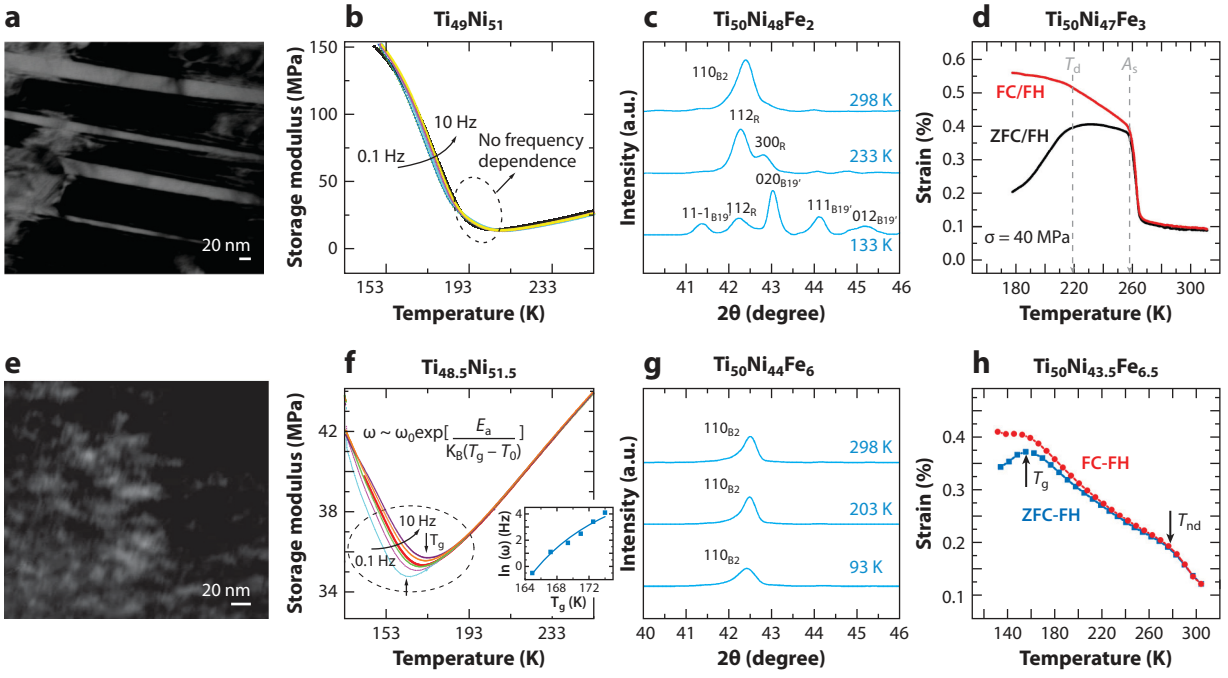

Figure 3

Comparison between experimental observations of the major characteristics of normal martensitic transformation (*a–d*) and strain glass transition (*e–h*). (*a*,*e*) Martensitic domain structures (*light gray*) from transmission electron microscopy observations. (*b*,*f*) Frequency dispersion of storage modulus from dynamic mechanical analysis measurements. The different colored lines represent different frequencies (0.1–10 Hz), the dashed circles indicate the dip positions in modulus without frequency dependence; the inset in panel *f* represents the fitting of frequencies ω and T_g (dip temperatures at different frequencies) by equation $\omega \sim \omega_0 \exp[\frac{E_a}{K_B(T_g - T_0)}]$. (*c*,*g*) Average crystal structures from X-ray diffraction at different temperatures. (*d*,*h*) Nonergodicity from ZFC/FC curves. T_g is the strain glass transition temperature, T_{nd} the transition temperature for the appearance of nanodomains of transformation strains, T_d the temperature indicating the maximum deviation change of ZFC curve from FC curve, and A_s the austenite transition start temperature. Abbreviations: FC, field cooling; FH, field heating; ZFC, zero field cooling. Panels *a*, *b*, *e*, and *f* adapted with permission from Reference 18; copyright 2005 American Physical Society. Panels *c*, *g*, and *h* adapted with permission from Reference 25; copyright 2010 Elsevier.

glass formation. More importantly, for martensitic systems having large transformation strains, point defects alone cannot suppress the martensitic transformation into a strain glass transition, no matter what the defect concentration is (49), and extended defects become necessary (30). For example, complex dislocation networks and substructures produced by cold rolling are found to have very strong impacts on martensitic transformations, even those having large transformation strains (50–53), leading to nearly linear SE without obvious stress plateaus and large loss energy.

Densely populated coherent nanoprecipitates can also suppress martensitic transformations into strain glass transitions (27, 54). However, with the increase of aging time and aging temperature, the system could change from strain glass transition to martensitic transition (28). Whether it is the concentration gradients in the matrix phase associated with the growing precipitates, coherency stress field generated by the precipitates, geometric confinement by the non-transforming precipitates, or all of the above (55, 56) that created the strain glass state is still unclear. More detailed experimental characterizations in combination with computer simulations are required to figure this out.

In addition, strain glass has also been reported in Ti-24Nb-4Zr-8Sn (Ti2448 for short), where both nanoscale concentration modulations (57, 58) and nanoscale shuffle domains (59) have been observed, both of which could have contributed to the formation of a strain glass state in the alloy. Similar transition behaviors to strain glass transition have also been reported in prestrained NiTi-Nb nanocomposite, where Nb nanowires are embedded in a NiTi SMA matrix (60). The prestraining produces plastic deformation in the Nb nanowire and introduces dislocations at the Nb nanowire and NiTi matrix interfaces, which harbor martensitic embryos that grow but are confined by neighboring Nb nanowires upon loading (61).

As mentioned in Section 1, strain glass and strain glass transition can be distinguished from normal martensite and martensitic transformation by their unique characteristics (**Figure 3**). Below, we present some detailed examples of these experimental characterization results.

2.1. Characterization of Strain Glass Microstructure

Strain glass can be defined as a disordered state with mottled or tweed nanoscale martensitic domains. The detailed characterization of the distribution of strain domains in a strain glass system is the key evidence needed to understand the physical origin of strain glass transition. To characterize the microstructure, the average structure in microscale and local structure in nanoscale are discussed in the following sections.

2.1.1. Average structure of a strain glass. Before the discovery of strain glass transition in SMAs, it was assumed that excess point defect doping completely suppresses martensitic transformation (62, 63) because XRD measurements did not show any structural changes. For example, $Ni_{50+x}Ti_{50-x}$ with $x \geq 1.5$ and $Ni_{50-x}Ti_{50}Fe_x$ with $x \geq 6$ have been reported as nontransforming materials (14, 64). However, the abnormal electrical resistivity change as a function of temperature and the diffuse scattering patterns observed in these materials have remained puzzles for a long time (65, 66). Nanodomains of transformation strains have been reported in these systems, and they have recently been confirmed to be strain glass systems (18, 19, 25, 34, 67). The average structure of a strain glass shows no split of diffraction peak caused by the martensitic phase but a broad peak in XRD (**Figure 3**), which leads to diffuse scattering in the diffraction pattern (25). These can be attributed to the small size of the martensitic domains.

2.1.2. Local structures in a strain glass. To explore the local structures of a strain glass, high-resolution TEM images have shown the appearance of nanodomains of martensitic phases, which grow continuously upon cooling, as shown in **Figure 4** (37). The martensitic nanodomains have irregular shapes due to the random spatial distribution of point defects and the random stress field associated with them (47, 68, 69). No internally twinned structures have been observed in these nanodomains. In other words, nanodomains of individual martensitic variants are the main characteristics of this strain glass state. However, recent computer simulations have shown that nanodomains of twinning martensite confined by nanoscale concentration modulations could also exhibit continuous transformation behavior and nearly linear SE (58), but direct experimental evidence remains to be seen. In most cases, the martensitic nanodomains have the same crystal structure (as shown by similar diffraction patterns) and transformation strains as those of regular martensite (25, 37). For shuffle-mode regulated strain glasses, the shuffle domains set the scale of the strain domains (59). In this case, the shuffle nanodomains transform to shear nanodomains upon cooling with a continuous increase of the shear value (59). In NiTi-based SMAs, there exists a two-step martensitic transformation (i.e., B2-R-B19′). In this case, strain glasses with local R structure can be produced by doping point defects, while strain glasses with local B19′ structure can be produced only by severe cold rolling (30).

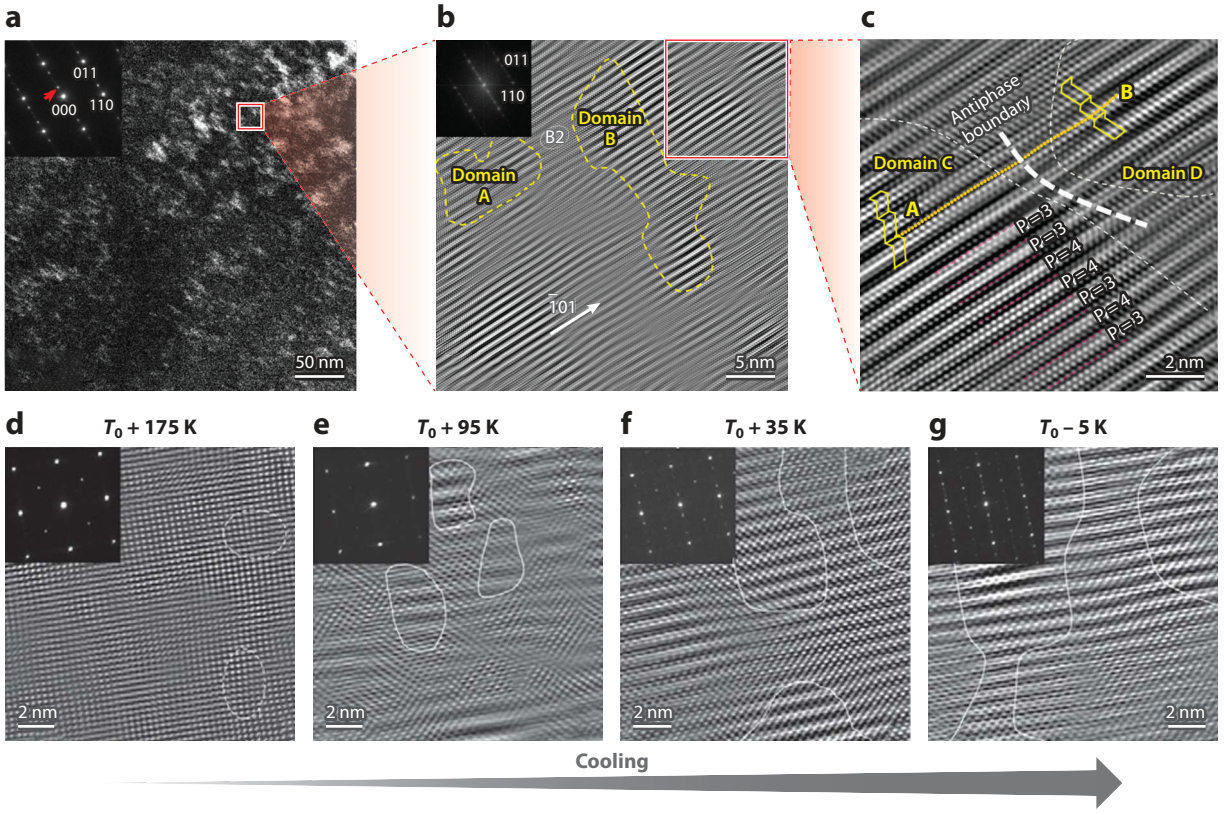

Figure 4

Nanodomain structure of strain glass in $Ti_{50}Pd_{41}Cr_9$. (*a*) Dark-field image obtained by using the reflection at the incommensurate 1/3 position (*red arrow* in the *inset*) showing nanodomains of individual martensitic variants. (*b*,*c*) High-resolution transmission electron microscopy images of different martensitic domains obtained from the incident zone; the inset in panel *b* is the fast Fourier transform pattern. The white arrow represents the [$\bar{1}$01] direction and yellow dotted circles represent the martensitic domains. A B2-like structure exists between the two domains. The dotted line in panel *c* represents the lattice change (i.e., shuffle) between two martensitic domains C and D with the formation of an antiphase boundary; the yellow steps represent the lattice modulation A and B due to different shuffle directions and P represents the stacking period for the lattice modulation, with P = 3 and P = 4 representing a period of three and four plane intervals, respectively. (*d*–*g*) In situ observation of microstructure evolution of martensitic nanodomains upon cooling. Insets show the corresponding diffraction patterns, white circles represent the regions of nanosized martensitic domains, and the gray arrow at the bottom describes the cooling direction. Figure adapted with permission from Reference 37; copyright 2014 American Physical Society.

The spatial confinements by local stress or concentration field (associated with random defects, spinodal decomposition, or precipitation) that form percolating networks (23, 24) leading to the formation of these nanodomains of individual martensitic variants are discussed in Section 3. These nanodomains nucleate and grow continuously upon cooling and may transform into long-range ordered twinning martensite (i.e., strain crystal) at a critical temperature that is a function of defect concentration. This phenomenon is reported as spontaneous strain glass to martensite transition (32, 70). Upon cooling, the volume fraction of a suppression field caused by defects decreases due to the increase of driving force for martensitic transformation, leading to the growth of martensitic nanodomains and the formation of normal martensites (23, 31). Isothermal martensitic transformations have also been reported in strain glass systems below the strain glass

transition temperature (T_g) (31, 32, 71, 72), which is due to the slow domain wall motion caused by defect pinning.

2.2. Characteristics of Strain Glass Transition

Conventional martensitic transition is a first-order transition accompanied by the formation of coarse twin structure, narrow transition temperature range, and large thermal hysteresis. The formation of nanoscale martensitic domains in strain glass implies a different transition mechanism from conventional martensitic transition to capture the strain glass transition behavior, the dynamic characteristic, the freezing process, and the thermal effect. These are discussed in the following sections.

2.2.1. Frequency dispersion in dynamic mechanical analysis. As a freezing process, all glass systems show relaxation behavior (73). The α relaxation, which is a general relaxation in different glass systems (including polymer glass, oxide glass, and metallic glass) (74–76), has also been observed in strain glass systems at T_g (18). In fact, frequency dispersion of storage modulus, loss modulus, and internal friction upon cooling measured by DMA has been used as a key indicator of strain glass transition in materials once called nontransforming. As mentioned in Section 2.1.2, in strain glass systems, martensitic nanodomains form and grow continuously upon cooling. These nanodomains have a size distribution, and domains of different sizes could respond differently to an applied alternating stress/strain field, resulting in frequency dispersion. When all the martensitic domains could follow the frequency of the alternating external stress/strain field instantaneously, the system shows pure elastic characteristics, and no internal friction could be observed. If some martensitic domains cannot follow the frequency of the external field instantaneously, the system shows viscoelastic characteristics and exhibits internal friction. For normal martensitic transformation, the transformation occurs within a narrow temperature range with rapid growth of martensite via autocatalysis, leading to instantaneous formation of relatively large martensitic domains. These domains show almost the same lag phase responding to the external field at the same frequency, and the lag phase changes with the change of the applied frequency in DMA. Thus, no obvious frequency dispersion can be observed upon cooling, but the system shows different internal friction values at different frequencies. For strain glass transition, autocatalysis is completely suppressed by the random field of defects, and martensitic nanodomains nucleate randomly and grow continuously upon cooling. This leads to a broader size distribution of the nanodomains. Nanodomains of different sizes have different response rates and lag phases at different frequencies and temperatures. Thus, the frequency dispersion of strain glass transition exhibits different responses in different martensitic nanodomains under alternating loading. From energetics, there exist numerous energy basins and minimum energy barriers (saddle points) among them on the free energy landscape in the transformation strain space (67, 77) due to the existence of random defects. Different saddle points correspond to different activation energy barriers for the evolution of the transformation strains, leading to different response rates and times and thus different frequency dispersions observed.

This frequency dispersion can be described well by the Vogel-Fulcher equation (78), which can be used to estimate the ideal T_g and activation energy. This time-dependent response suggests the possibility of isothermal transformations. Accordingly, experimental observations have shown an isothermal transition from strain glass to martensite at a critical defect concentration (31, 71), which can be attributed to the competition between the driving force for martensitic transformation and the random field from defects that suppress the martensitic transformation. Upon cooling, the driving force increases and the suppression field from defects shrinks. Unlike athermal nucleation and growth by autocatalysis in conventional martensitic transition (79), the

evolution of martensitic nanodomains in strain glass transition into internally twinned martensitic plates within a certain temperature range and a defect concentration range is time dependent (23). Due to the relatively faster movement of lattice shear (a diffusion-less process) compared to atomic diffusion in conventional glass, strain glass transition shows an atypical, colder-is-faster feature (33), and spontaneous strain glass to martensite transition has been reported upon cooling in strain glass systems within certain ranges of defect concentration (70, 80). The increased driving force for martensitic transformation upon cooling can overcome the energy barrier for martensitic growth created by defects, and the system transforms into normal martensite. Similar spontaneous transition phenomena have been reported in relaxor ferroelectrics as well (81, 82). Such a spontaneous strain glass to strain crystal (martensite) transition can occur within local regions, which offers an opportunity to design heterogeneous domain structures, including both microscale and nanoscale ferroelectric or ferroelastic domains with good comprehensive properties (83).

2.2.2. Nonergodicity in zero-field cooling and field cooling. Nonergodicity is also an important feature of a glass transition, which is characterized by a history dependence of the order parameters (e.g., strain, polarization, and magnetization) in response to an external field. Experimentally nonergodicity is revealed by samples having two different cooling histories (zero-field cooling and field cooling) showing two different evolutions of the order parameter (strain) during a heating process under a fixed external stress (i.e., field heating), as shown in **Figure 3*b*** (84). A microscopic picture of such a disparity in the field-heating curves between the zero-field-cooled and field-cooled samples is as follows. For a zero-field-cooled sample, which is characterized by random nanodomains, upon field heating from the $T \ll T_g$, the macroscopic strain value gradually increases as the size of the martensitic nanodomains gradually decreases; thus, some nanodomains could respond to the external stress by domain switching. When the temperature rises above T_g, the volume fraction of the martensitic domains decreases rapidly, leading to a decrease in the response strain. Thus, the zero-field-cooling and field-heating curves show a hump (**Figure 3*b***). The peak temperature corresponds to the freezing temperature, T_g, in strain glass transition. For a field-cooled sample, it shows larger strain values at low temperatures ($<T_g$) because of the aligned (or textured) nanodomains by the applied field. Upon heating ($>T_g$), the volume fraction of martensitic nanodomains decreases continuously, leading to a continuous decrease of strain. The strain difference between the field-cooling-field-heating curves and the zero-field-cooling-field-heating curves decreases due to the decrease in the volume fraction of the martensitic nanodomains (**Figure 3*b***). The two curves start to overlap at a critical temperature, defined as T_{nd}, at which the martensitic nanodomains disappear or appear upon heating or cooling.

It should be noted that a normal martensitic transformation (and many solid-state phase transformations) also shows a breaking of ergodicity at $T < M_s$ as a result of the frozen status of microscale strain domains (i.e., internally twinned martensite), but to a lesser extent, as the zero-field-cooling and field-cooling curves are essentially overlapping at $T > A_s$ (the start temperature of inverse transformation to austenite) (**Figure 3*d***). This is different from a strain glass transition.

2.2.3. Heat flow and electrical resistivity in strain glass transition. The strong first-order martensitic transformation shows a typical exothermic peak upon cooling and an endothermic peak upon heating because of the latent heat of transformation. The exothermic and endothermic peaks occur at different temperatures, which implies the existence of thermal hysteresis, typical for a first-order transition. Unlike normal martensitic transformations, however, the strain glass transition shows no obvious exothermic and endothermic peaks upon cooling and heating but rather shows a clear heat capacity hump without thermal hysteresis (18, 25, 34). This suggests that the strain glass transition is a high-order-like (higher than second order) continuous transition

process. Note that such a continuous transformation could be attributed to an integral effect of many local first-order martensitic transformation events that occur at different temperatures or stresses (i.e., broadly smeared multiple first-order transitions). An exception to this could be the shuffle-mode regulated strain glass transition found in Ti2448 mentioned in Section 2 (59), in which the shuffle nanodomains transform to shear nanodomains upon cooling with a continuous increase of the shear value.

It is interesting to note that the strain glass state was discovered when people were seeking answers to the experimentally observed abnormal electrical resistivity change in the so-called nontransforming NiTi-based alloys (63, 65, 66). Due to the disappearance of heat flow peaks in DSC curves, it was assumed that there is no transformation in TiNi and TiNiFe systems when the doped Ni and Fe concentrations, respectively, are high. If there are no phase transformations in metals, their electrical resistivity should decrease with decreasing temperature. However, the electrical resistivity of these systems shows abnormal increases upon cooling (63, 65, 66). This abnormal electrical resistivity increase has been thought to be associated with the appearance of a precursory martensitic phase, but no normal martensitic transformation has been reported upon further cooling. The R martensitic phase in these alloys has higher electrical resistivity than that of the B2 parent phase. Thus, the abnormal electrical resistivity increase with decreasing temperature must be related to the B2 to R transformation, which has been proved to be a strain glass transition that produces R-phase nanodomains in the doped TiNi and TiNiFe systems (25, 34). The continued nucleation and growth of R martensitic nanodomains upon cooling lead to an abnormal increase in the electrical resistivity. Experimental observations have shown that the temperature range in which the abnormal electrical resistivity is observed is consistent with the temperature range in which the frequency dispersion of the storage modulus occurs and the divarication of the zero-field-cooling and field-cooling curves starts. In particular, the electrical resistivity has shown a continuous increase with zero thermal hysteresis upon cooling and heating, which is different from how the electrical resistivity changes during normal B2 $\rightleftharpoons$ R martensitic transformation (85). The inflection point on the electrical resistivity curves upon cooling at high temperature is related to the special temperature, T_{nd}, at which stable martensite nanodomains start to appear, while the inflection point at low temperature is related to T_g (25). Note that the strain glass transition with B19′ local structure shows a continuously decreasing electrical resistivity upon cooling, which is due to the lower value of electrical resistivity of the B19′ phase compared to that of the B2 phase (86).

2.3. Phase Diagram (Strain State Diagram) of Strain Glass System

According to the above experimental measurements, phase diagrams of different strain states, including strain liquid (i.e., the parent phase), strain crystal (i.e., the normal martensite phase), strain glass, and transitions among them, have been established in different SMAs (6, 25, 26, 34, 35, 44). **Figure 1** shows such a phase diagram. At low defect concentrations, there exist normal martensitic transformations between strain liquid and strain crystal, with the formation of microscale, internally twinned martensite upon cooling. At high defect concentrations, however, such martensitic transformations are replaced by strain glass transitions with continuously freezing-in martensitic nanodomains. Besides the martensitic transformations and strain glass transitions shown in **Figure 1**, further experiments and simulations have shown that the phase boundary between the strain crystal and strain glass is not vertical but tilted and is not a single line but a region, which indicates a narrow concentration range in which strain glass transition and martensitic transformation could coexist (32, 70, 71, 80, 87). Within this concentration range, the systems show the coexistence of microscale, long-range ordered, internally twinned martensitic

plates at some local regions and martensitic nanodomains at some other local regions. The DMA measurement shows two peaks for the storage modulus and internal friction, and the XRD results show the conventional peak for the martensitic phase (32, 70).

Above T_g at a high defect concentration or above M_s at a low defect concentration and below T_{nd} (see **Figure 1**), there exists a precursory strain state over a wide concentration range. This partially frozen state contains both static (frozen) and dynamic (unfrozen) nanodomains of martensite. The dynamic nanodomains of martensite, which can further transform into normal martensite, are also called tweed structure in systems with large elastic anisotropy (19, 88). Thus, in a ferroelastic system, the phase transitions change from a strong first-order martensitic transformation to a continuous strain glass transition with increasing defect concentration. Different defect types will create different amounts of lattice distortions and alter the phase boundaries in the phase diagram (23, 49). For example, 1.5% excess Ni is required in NiTi and 6% Fe is required in NiTi-Fe to induce a similar strain glass transition.

The establishment of strain glass phase diagrams has expanded the theory of phase transformations in ferroelastic systems and could provide (*a*) a new angle from which to look at some long-standing, unresolved issues, such as nearly linear SE, the disappearance of normal martensitic transformation heat flow peaks, and Invar and Elinvar anomalies, and (*b*) useful guidance for defect engineering to achieve desired strain domain patterns for controlled strain release.

2.4. Unique Properties of Strain Glass Systems

Because of the continuous transition characteristic, strain glass systems have well-controlled strain release during deformation and may offer many unique properties, such as linear SE with nearly zero hysteresis (69), excellent thermal cycling properties with strong fatigue resistance (30), and Invar and Elinvar anomalies (5, 6).

Figure 5*a* shows a typical example (30) of nearly linear SE (no strain avalanche) with a slim hysteresis and high strength over a wide temperature range, which has been observed in most strain glass systems. Continuous elastic modulus softening upon cooling associated with the strain glass transition compensates for the normal modulus hardening upon cooling and leads to the Elinvar anomaly (5, 7, 89) (see, e.g., **Figure 5*b***), while tunable strain release of strain glass transition leads to a tunable thermal expansion coefficient that is positive, negative, or close to zero (i.e., the Invar phenomenon) (6, 90, 91) (see, e.g., **Figure 5*d***). Large magnetostriction has also been reported in the Fe-Pd strain glass system (see **Figure 5*c***), which is caused by the ease with which martensitic nanodomains switch (45, 92). SE with low modulus could have important applications in accurate control of microelectromechanical systems and pediatric implants, the wide temperature range for SE may be suitable for space exploration, and Invar and Elinvar strain glasses can be used in high-precision instruments. Note that strain glasses in NiTi SMAs also show normal SME and SE with large hysteresis at low temperatures (approximately 173 K), which can be attributed to stress-induced R strain glass to B19′ martensite transition (93).

3. THEORETICAL MODELS AND COMPUTER SIMULATIONS OF TRANSFORMATIONS AMONG DIFFERENT STRAIN STATES

In experiments, strain glass has shown unique nanoscale martensitic domains and continuous transition behavior, and it is believed that defects play an important role in regulating the transition behavior and producing disordered strain state. To explain the physical origin of strain glass transition and nanoscale martensitic domains, many models, from atomic scale to mesoscopic scale, are reviewed in the following sections.

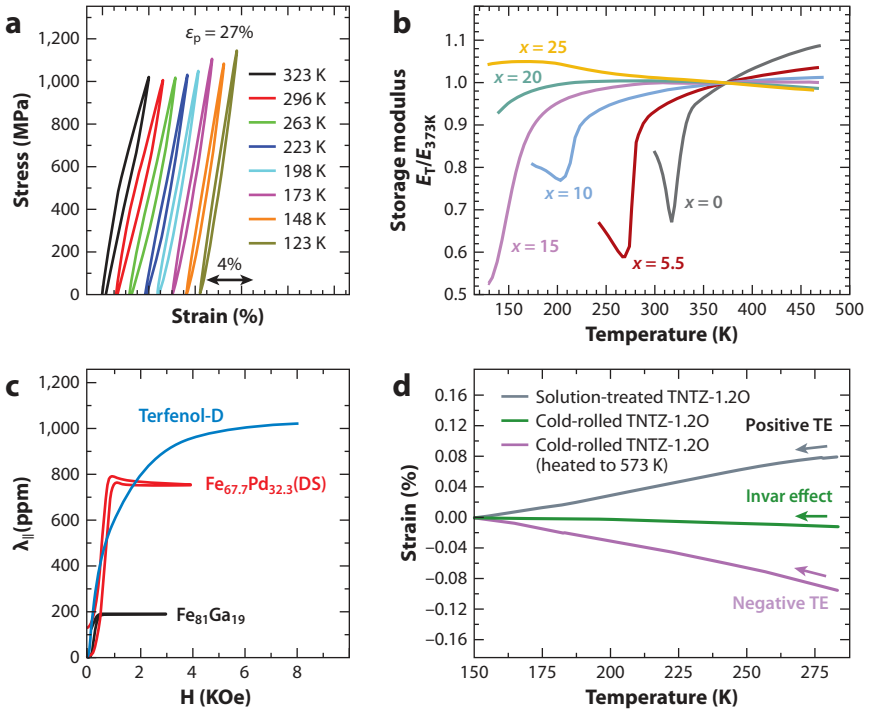

Figure 5

The unique properties of strain glass systems. (*a*) Superelasticity with narrow hysteresis over a wide temperature range in a B19′ strain glass produced by cold rolling of $Ti_{49.2}Ni_{50.8}$ with $\varepsilon_p = 27\%$. (*b*) Elastic modulus at different temperatures for $TiNi_{50-x}Co_x$ in which strain glass transitions have been confirmed when $x > 15$. (*c*) Magnetostriction in $Fe_{67.7}Pd_{32.3}$ strain glass. (*d*) Invar for cold-rolled TNTZ-1.2O (at. %) (5, 6, 30, 45) along the rolling direction. Arrows represent the cooling process. Abbreviations: DS, directionally solidified alloys; ε_p, thickness reduction; TE, thermal expansion; TNTZ, Ti-23Nb-0.7Ta-2Zr. Panel *a* adapted with permission from Reference 30; copyright 2017 American Physical Society. Panel *b* adapted with permission from Reference 5; copyright 2005 American Institute of Physics. Panel *c* adapted with permission from Reference 45; copyright 2017 American Physical Society. Panel *d* adapted from Reference 6 (CC BY-NC-ND 3.0)

3.1. Theoretical Models of Strain Glass Transition

To understand the experimentally observed unique phenomena and properties associated with strain glass transition, several models have been proposed that consider the local stress field caused by random point defects; local concentration and stress fields generated by nanoprecipitates; the elastic anisotropy of different systems; the strain network created by different defects including point defects, dislocations, and nanoprecipitates; and other characteristics (23, 24, 47, 68, 94). Adding random, stress-carrying defects could interrupt the formation of long-range ordered transformation strain patterns because a random stress field is incompatible with the long-range ordered, self-accommodating strain patterns produced by normal martensitic transformations via autocatalysis. In addition, local solute concentration variations associated with either impurity doping, spinodal decomposition, precipitation, and segregation at extended defects create thermodynamic stability (i.e., M_s) variations. As a consequence, different locations in the system start the martensitic transformation at different temperatures or stress levels, with isolated nanodomains of martensite formed in regions with high M_s being confined by the surrounding parent phase

matrix that has higher stability (58, 68, 95). This also suppresses the autocatalysis and smears the martensitic transformation into a strain glass transition.

Furthermore, the stress-free transformation strain and elastic anisotropy of the system itself also influence how easily strain glass forms (47, 48, 96). A smaller transformation strain or lower elastic anisotropy requires a lower defect concentration or a weaker local field at a fixed defect concentration, and a larger transformation strain or a higher elastic anisotropy requires a higher defect concentration or a stronger local field at a fixed defect concentration, to convert normal martensitic transformations into strain glass transitions.

Phase field modeling based on Landau theory of phase transformations has been used widely in the study of martensitic transformations (97, 98) and strain glass transitions (23, 68, 69), which can incorporate easily both the chemical and mechanical effects discussed above [i.e., effects from concentration and stress fields associated with various point defects (22, 47, 49, 68, 94, 99–101) and extended defects such as nanoprecipitates (27, 28, 55, 58, 102, 103) and dislocations (61, 104–107)]. The total free energy of the system in the phase field model consists of four parts:

$$F = \int d^3r[f_{\rm ch} + f_{\rm L} + f_{\rm gr}] + E_{\rm el}, \qquad 1.$$

where $f_{\rm ch}$ is the chemical free energy density, which is usually approximated by a Landau polynomial (94, 97),

$$f_{\rm ch}(\mathbf{r}, c, T) = f^0(c, T) + \frac{1}{2}B_2(\mathbf{r}, c, T)\left(\sum_p^n \eta_p^2\right) - \frac{1}{4}B_4(\mathbf{r}, c, T)\left(\sum_p^n \eta_p^4\right) + \frac{1}{6}B_6(\mathbf{r}, c, T)\left(\sum_p^n \eta_p^2\right)^3, \qquad 2.$$

where $\mathbf{r}$ is the spatial coordinate, c is the point defect concentration, T is the temperature, $\eta_{\rm p}(\mathbf{r})$ $(p = 1, 2, \ldots, n)$ are the structural order parameters that characterize the martensitic phase with stress-free transformation strain of the $p^{\rm th}$ variant from total n variants, $B_2 = B_2{}^0[T - T^0(c)]$, $T^0(c) = T^{00} + bc$ with T^{00} being the phase transition temperature of a defect-free system, and b is a constant that characterizes the concentration effect on the transition temperature. The excess energy density $f_{\rm L}$ associated with a local stress field generated by defects is characterized by (68, 69)

$$f_{\rm L} = -\sigma^{\rm L}(\mathbf{r})\varepsilon(\mathbf{r}), \qquad 3.$$

where $\sigma^{\rm L}(\mathbf{r})$ is the local stress field created by defects [which has different forms for different types of defects, such as point defects (substitutional and interstitial point defects may also assume different forms), dislocations, and coherent precipitates] and $\varepsilon(\mathbf{r})$ is the strain field associated with the martensitic domains described by the structural order parameters $\eta_p(\mathbf{r})$ and the stress-free transformation strain ε_p^{00} [i.e., $\varepsilon(\mathbf{r}) = \sum_p^n \varepsilon_p^{00}(\mathbf{r})\eta_p^2(\mathbf{r})$] (68, 97, 98). Also, $f_{\rm gr}$ is the gradient energy density associated with structural heterogeneity characterized by $\eta_p(\mathbf{r})$, $f_{gr} = \frac{1}{2}\beta(\sum_p^n \nabla\eta_p)^2$, where β is the gradient energy coefficient, and $E_{\rm el}$ contains the coherency elastic strain energy and work term by external stress, which can be described by Khachaturyan's microelasticity theory (97, 98):

$$E_{el} = \frac{1}{2}C_{ijkl}\sum_{p=1}^n\sum_{q=1}^n \varepsilon_{ij}^{00}(p)\varepsilon_{kl}^{00}(q)\int \eta_p^2(\mathbf{r})\eta_p^2(\mathbf{r}) - \frac{1}{2}\sum_{p=1}^n\sum_{q=1}^n \int \frac{d^3\mathbf{k}}{(2\pi)^3}B_{pq}(\mathbf{e})\{\eta_p^2(\mathbf{r})\}_k\{\eta_q^2(\mathbf{r})\}_k^* - \int \sigma_{\rm appl}\sum_{p=1}^n \varepsilon_p^{00}(\mathbf{r})\eta_p^2(\mathbf{r})d^3r, \qquad 4.$$

where C_{ijkl} is the elastic constant tensor, $\mathbf{k}$ is the wave vector defined in the reciprocal space, $\{\eta_p^2(\mathbf{r})\}_k$ is the Fourier transform of $\eta_p^2(\mathbf{r})$, $\{\eta_q^2(\mathbf{r})\}_k^*$ is the complex conjugate of $\eta_q^2(\mathbf{r})$ and $B_{pq}(\mathbf{e}) = e_i\sigma_{ij}^0(p)\Omega_{jk}\sigma_{kl}^0(q)e_l$, $\sigma_{ij}^0(p) = C_{ijkl}\varepsilon_{ij}^{00}(p)$, $\Omega^{-1} = C_{ijkl}e_ke_l$, and σ_{appl} is the applied external stress.

The microstructural evolution during martensitic transformation is then characterized by the time-evolution of the structural order parameters, $\eta_p(\mathbf{r})$, following the time-dependent Ginzburg-Landau equation:

$$\frac{\partial \eta_p(\mathbf{r},t)}{\partial t} = -L\frac{\delta F}{\delta \eta_p(\mathbf{r},t)} + \xi(\mathbf{r},t), p = 1,\ldots,n, \qquad 5.$$

where L is the kinetic coefficient characterizing domain wall motion and ξ is the Langevin noise term describing thermal fluctuations.

3.1.1. Role of point defects. The first strain glass system discovered and most of the strain glass systems reported so far are R-phase strain glasses created by point defect doping. Similar to the effects of point defect doping on the formation of spin glasses and relaxors in ferromagnetics and ferroelectrics, point defect doping also has strong impacts on M_s, martensitic transformation product, and martensitic transformation path in ferroelastic systems (14). Three important effects from random point defects on martensitic transformation have been identified (68, 94, 95). The first is the global transition temperature effect (GTTE) associated with alloy composition change by point defect doping, which influences the overall transition temperature of the alloy as a whole. Second, the local transition temperature effect (LTTE) is associated with local composition variation created by the random spatial distribution of impurities, which creates a local transition temperature variation (because M_s is a sensitive function of composition). Finally, the local field effect (LFE) is caused by a local stress/strain field associated with local lattice distortion created by the point defects, which influences local M_s and what variants of martensite form (i.e., variant selection).

Both GTTE and LTTE are chemical effects and can be accounted for by the local chemical free energy in Landau theory [e.g., they can be captured by altering the expansion coefficient B_2 in Equation 2 with $B_2 = B_2{}^0(T - T^{00} + bc)$]. When $c = \overline{c(\mathbf{r})}$, the equation describes GTTE, whereas when $c = c(\mathbf{r})$, the equation describes LTTE. The LFE is a mechanical effect, as shown in Equation 3, and can be characterized by the elastic interaction between a martensitic domain characterized by its transformation strain ε_p^{00}, order parameter η_p, and the local stress field σ^{L} created by the point defects. **Figure 6*a*** shows the effects of the LFE from lattice distortion caused by a point defect.

Phase field simulations (23, 68, 69) based on the above established Landau free energy model could describe the formation of martensitic nanodomains, zero-field-cooling/field-cooling curves, frequency dispersion, and continuous transition behavior of strain glass transitions (23, 68, 69). Based on the simulation results, phase diagrams of the strain glass systems studied have been established (23, 68) that are consistent with the phase diagram shown in **Figure 1** and experimentally determined ones (25, 26, 34). **Figure 6*b*** shows an example of 2D phase field simulation results of martensitic transformation and strain glass transition in a model system that has a cubic to tetragonal martensitic transformation. When the defect concentration is low ($c = 0.0$–0.1), the system shows a normal martensitic transformation that produces long-range ordered twinning martensite. However, when the defect concentration exceeds a critical value (e.g., $c = 0.125$ in this example), the long-range ordered twin structures are replaced by frozen tweed structures consisting of nanodomains of individual martensitic variants (a typical strain glass microstructure). The nanodomain size decreases with increasing defect concentration. **Figure 6*c*,*d*** shows the simulated microstructural evolution and related volume fraction change

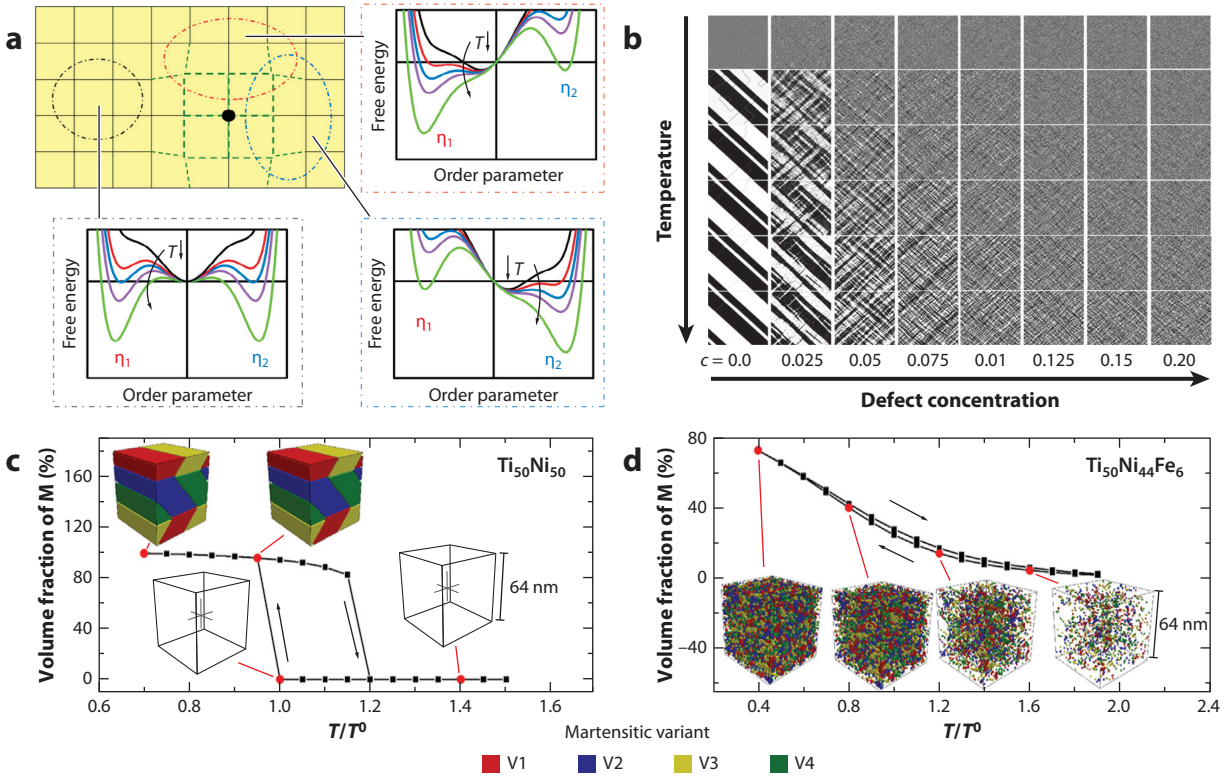

Figure 6

(*a*) Effects of a lattice defect (*black dot*) on lattice distortions at different locations and the corresponding free energy curves at these locations at different temperatures. An undistorted location is also shown for comparison. The black line and black circle represent the normal lattice without distortion; the green line and red and blue circles represent distorted lattices. The arrows point to the corresponding free energy curves at different temperatures (*downward arrow* represents decreasing temperature); *T* represents temperature and η_1 and η_2 represent the order parameters for two different martensitic variants. (*b*) Two-dimensional phase field simulation results of microstructure evolution upon cooling at different defect concentrations ($c = 0.0$–0.2). Gray represents the austenite and black and white represent two different variants of the martensite. (*c*,*d*) Three-dimensional phase field simulation results of the martensitic volume fraction changes upon cooling and heating for (*c*) normal martensitic transformation and (*d*) strain glass transition (68, 69). The black arrows represent cooling and heating, the four colors represent four martensitic variants, and the transparency represents the parent phase. Panels *a* and *b* adapted with permission from Reference 68; copyright 2010 American Physical Society. Panels *c* and *d* adapted with permission from Reference 69; copyright 2014 Elsevier.

for B2 to R martensitic transformation in $Ti_{50}Ni_{50}$ and B2 to R strain glass transition in $Ti_{50}Ni_{44}Fe_6$, respectively, upon cooling and heating (69). The normal martensitic transformation in **Figure 6*c*** shows a sudden appearance and rapid growth of martensite into a long-range ordered, internally twinned, herringbone structure within a narrow temperature range upon cooling. These martensitic twin structures transform to austenite at a higher temperature upon heating, leading to a large hysteresis. However, the strain glass transition in **Figure 6*d*** shows continuous appearance/disappearance and slow growth/shrinking of individual martensitic domains over a wide temperature range upon cooling/heating, with a nearly vanishing hysteresis.

3.1.2. Defect strength and strain glass transition. The critical value of defect concentration for separating martensitic transformation and strain glass transition may change as the type of point defect (e.g., substitutional versus interstitial, impurities of different atomic sizes and

different chemical similarities to the host atoms) changes. In the NiTi-Cu system, for example, doping approximately 15% Cu still cannot suppress normal B2 to B19 martensitic transformation, while doping 7% Ni is enough to change B2 to B19 martensitic transformation to B2 to R strain glass transition with the formation of R-phase nanodomains (35). These subtle differences could be captured by adjusting their chemical and mechanical effects in the Landau free energy model discussed in Section 3.1.1. Among GTTE, LTTE, and LFE, the latter seems to play the most important role in suppressing autocatalysis, interrupting long-range ordered strain domain patterns assumed by self-accommodation among different martensitic variants, and turning a normal martensitic transformation into a strain glass transition (49). This is because self-accommodation and autocatalysis are all caused by long-range elastic interactions among different martensitic variants (i.e., mechanical in origin), and LFE (also mechanical in origin) makes its own variant selection that is most likely incompatible with the variant selection process by self-accommodation. Thus, among the three effects, the LFE provides the strongest suppression field resisting the formation of long-range ordered domain patterns.

For example, cold rolling alone (in which only the LFE associated with dislocations is present) can make B19′ (approximately 10% transformation strain) strain glass transition in NiTi (30), while point defect doping alone (in which GTTE, LTTE, and LFE are present, but the LFE is rather weak) can only make R-phase (approximately 1% transformation strains) strain glass in NiTi-based SMAs, regardless of the defect concentrations (25, 26, 34, 108). Thus, weak LFE caused by point defects cannot induce the formation of strain glass with large transformation strains such as B19 or B19′ strain glasses. To design strain glasses with giant superelastic strains, stronger LFE from extended defects such as dislocations is required (49). However, large and asymmetrical (nondilatational) lattice distortions caused by interstitial atoms can produce strain glass with intermediate transformation strain (approximately 2.6%)—for example, in oxygen-doped TiNb-based alloys (6, 59, 109).

3.1.3. Effect of elastic anisotropy. Since the order parameter of strain glass is the transformation strain, the long-range elastic interactions between nucleating martensitic domains and defects as well as among different martensitic domains themselves play a dominant role in the energetics of strain glass formation, which is similar to the case of normal martensitic transformations. In particular, the interplay among the activation energy barrier for nucleation of a single, non-self-accommodated martensitic variant at defects, the activation energy barrier for the formation of a self-accommodating multivariant martensitic twin, and the local chemical driving force for martensitic transformation determines the thermal stabilities of strain glass, strain crystal, and strain liquid.

Reference 47 reported that the elastic anisotropy of a system could influence the transformation strain domain patterns, as shown in **Figure 7**. The elastic anisotropy factor A can be defined as $A = C_{44}/C' = A_3/A_2$, where $A_2 = 2C' = C_{11} - C_{12}$ and $A_3 = C_{44}/2$. The decrease of elastic anisotropy A_3 could change the martensitic transformation behavior and microstructural evolution. **Figure 7** shows that a high elastic anisotropy could favor the formation of tweed at high temperature and long-range ordered twinning martensite at low temperature (88, 110), while a low elastic anisotropy prefers the formation of nanodomains [i.e., a strain glass state (18, 19)]. However, a pure martensitic system with elastic isotropy alone cannot produce strain glass (98); randomly distributed defects with enough concentration are still necessary. The anisotropy may change the value of the critical defect concentration required to form a strain glass, which is similar to the effect of different types of point defects.

3.1.4. Role of extended defects. As discussed above, point defects could suppress a normal martensitic transformation into a strain glass transition only when the transformation strain is

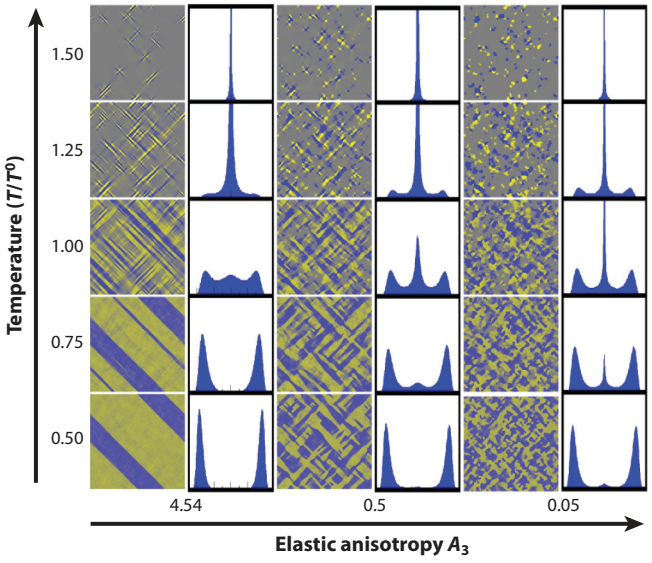

Figure 7

Effect of elastic anisotropy A_3 on microstructure evolution obtained from 2D phase field simulations. The yellow and blue colors represent two martensitic variants, and the gray color represents the austenite phase. The picture to the right of each microstructure represents the local strain distribution; the center peak represents the zero strain, and the peaks on both sides represent the strain of two martensitic variants. The elastic anisotropy A_3 (i.e., $C_{44}/2$) changes from 4.54 to 0.05 and the relative temperature changes from 0.5 to 1.5. Figure adapted with permission from Reference 47; copyright 2008 American Physical Society.

small. For example, although R, B19, and B19′ martensitic phases have been observed in NiTi-based systems, only R-phase (trigonal) strain glass has been reported by doping point defect (25, 26, 34). No B19 or B19′ strain glasses can be generated by doping point defects in NiTi-based SMAs. This is because the transformation strains of the B19 (approximately 8%) and B19′ (approximately 10%) phases are much larger than that of the R phase (approximately 1%) (14). Point defects create limited lattice distortions with weak LFE, which cannot suppress the autocatalytic nucleation and growth of B19 or B19′ martensitic domains. Now the question is whether stronger defects could make B19 or B19′ strain glasses.

Like point defects, extended defects such as dislocations, precipitates, and grain boundaries could also produce local composition variations and lattice distortions, which should show LTTE and LFE. However, unlike point defects, whose LFE is rather limited, the LFE associated with extended defects could be much stronger. Densely populated dislocations, deformation twins, and amorphous domains have been observed in severely cold-worked NiTi SMAs (111, 112), which have indeed resulted in the change from a normal B2 to B19′ martensitic transformation to a B2 to B19′ strain glass transition (29, 30). Such a B19′ strain glass has shown a much larger recoverable strain (4%) within a wide temperature range (30) compared to that of the R strain glass (0.5%) (69). This can be attributed to the large transformation strain (approximately 10%) of the B19′ martensite. Local stress fields created by dislocations could induce martensitic embryos at temperatures above the M_s of the non-cold-rolled samples. For example, phase field simulations have shown that the stress/strain network created by dislocations produces embryonic martensitic domains at dislocations (61, 105). **Figure 8** shows the evolution of the martensitic domains under loading for a sample that has been plastically deformed to 5% strain before the loading, where

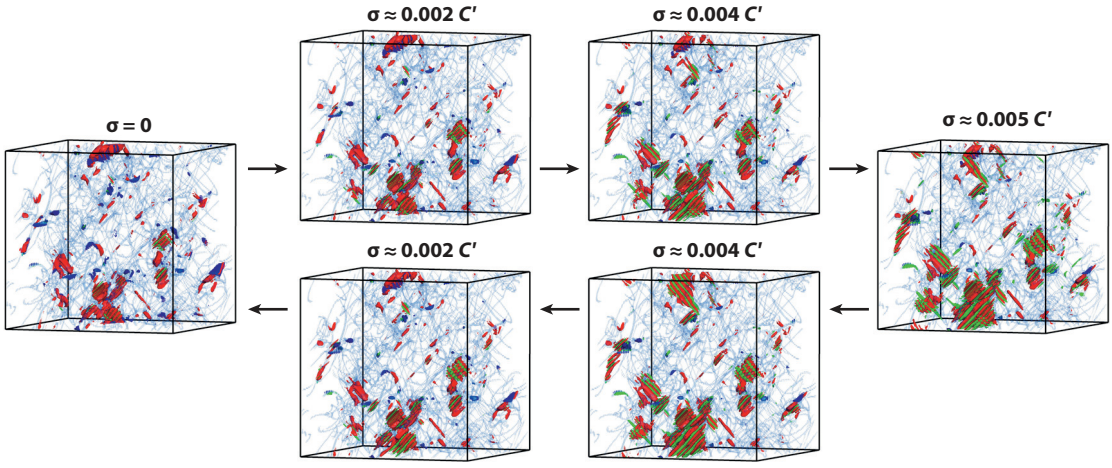

Figure 8

Phase field simulation of the evolution of nanoembryonic martensitic structures in Fe-30 at. % Ni with 5% plastic deformation under loading and unloading. The applied stress σ is equal to 0.0–0.005 C′, where $C' = (C_{11} - C_{12})/2$ and C_{11} and C_{12} are the elastic constants of the calculated system. The arrows to the right represent the loading process, and the arrows to the left represent the unloading process. The dislocation lines are in light blue, the parent phase is transparent, and the other colors describe different variants of martensite (105). Figure adapted from Reference 105 (CC BY 4.0).

martensitic domains exist above M_s and continue to grow upon loading. To be able to suppress autocatalysis completely and turn a normal B19′ martensitic transformation into a B19′ strain glass transition, a critical amount of cold work (i.e., a critical dislocation density) is required (61, 105). In addition to dislocations, deformation twin boundaries were also found to have the ability to harbor martensitic embryos (113–115).

These martensitic embryos induced by dislocations and deformation twins could grow instantaneously and continuously upon cooling/loading without the need for overcoming the activation energy barrier for nucleation, which reduces the hysteresis and increases the temperature range for SE (60, 61). Thus, dislocations and deformation twins could be more effective defects to produce strain glasses in different SMAs due to their strong LFE. Stress and temperature cycling of SMAs could also produce dislocations and deformation twins, which significantly impact the martensitic transformation behavior (116–118). For SE in SMAs, the critical stress for a stress-induced martensitic transformation has to be lower than that of stress-induced dislocation slip (14). The dislocations and deformation twins introduced by cold work and stress/temperature cycling increase the strength of the parent phase and hence enhance the SE of a strain glass system.

Precipitate phases having different structures and compositions from the parent matrix phase could influence the martensitic transformation path and martensitic transformation temperature because the precipitation reactions generate composition heterogeneity at the scale of the growing precipitates and the local stress field (for coherent precipitates) and impose geometrical confinement (since the precipitates do not transform) (55, 56, 103, 119–121). In NiTi-based SMAs, Ni_4Ti_3 precipitates can induce R phase and improve SE through strengthening the matrix (56, 121, 122), but no strain glass state or nano-sized martensitic domains have been reported in these alloys. As discussed in Section 2, the density of precipitates should play an important role in strain glass formation. The size and density of precipitates depend on alloy composition and aging temperature and time. Recent experimental work has shown that nanoprecipitates with high density by aging at a low temperature for a short time could induce strain glasses (27, 28). Unfortunately,

such nano-sized precipitates in NiTi SMAs can only induce strain glasses with local R structure. The lattice distortion caused by the precipitates is insufficient to induce B19 or B19′ strain glasses.

3.1.5. Atomic-scale understanding of strain glass transition. The above Landau theory is phenomenological, and the corresponding phase field simulations are at mesoscale. To gain a fundamental understanding of strain glass transition at the atomic scale, atomistic simulations are desired. Molecular dynamics (MD) simulations of phase transformations in NiTi systems have shown strain glass transition at high defect concentration, revealing that lattice distortion created by the Ni-Ni and Ni-Ti nearest neighbor atomic pairs at high antisite Ni concentrations leads to the suppression of autocatalysis and converts the martensitic transformation into a strain glass transition. The radial distribution functions of the bond length of Ni-Ni and Ni-Ti atomic pairs in a frozen strain glass state are closer to those in the martensitic phase, while the corresponding radial distribution functions in the unfrozen strain nanodomain states (i.e., tweed) are similar to those in the austenitic phase (123). In addition, first-principle calculations also suggest that the strain glass state may not be created by transformation strain pinning by point defects but rather by a disruption of the underlying electronic instability due to lattice expansion caused by the point defects (Co randomly substitutes Ni in this study) (124). Co atoms on the Ni sublattice lead to the formation of resonance (local) states and disrupt Fermi surface nesting.

Furthermore, the formation of strain glass has been attributed to the gradual percolation of local strain clusters (23, 24). Point defects create localized strain clusters that expand and reach a percolation threshold at the glass transition temperature (i.e., the strain clusters form a percolated strain network) as the defect concentration increases. For example, it has been shown that the local strain field created by point defects first forms isolated strain islands at high temperatures (**Figure 9*a***, **subpanel *i***). Upon cooling, these islands expand to anisotropic shape (due to elastic anisotropy) and form a percolated strain network (**Figure 9*a***, **subpanel *ii***), which constrains the nucleation and growth of martensitic domains at a low temperature, as shown in **Figure 9*a***, **subpanel *iv***. Further studies suggested that this strain network can interrupt the formation of long-range ordered strain domains such as those seen in internally twinned martensite because the so-called strain network is not compatible with the self-accommodating strain domain patterns. This effect can be quantified by calculating the suppression field through the elastic interaction energy $[f_L^p(\mathbf{r})]$ between the p^{th} variant of the martensite formed and the local stress field from the defects. The energetic criterion of the suppression field, $f_{\text{sup}} = f_L^p(\mathbf{r}) + f_{cb}(\mathbf{r})$, that determines whether a p^{th} martensitic variant could form and grow, can be written as $f_L^p(\mathbf{r}) + f_{cb} > 0$, or $f_L^p(\mathbf{r}) + f_{cb}(\mathbf{r}) > f_L^q(\mathbf{r}) + f_{cb}(\mathbf{r}), (p \neq q)$, where $f_{cb}(\mathbf{r})$ is the chemical driving force for the martensitic transformation (23). This means that either the parent phase or other variants of the martensitic phase will be more stable and the formation of the p^{th} martensitic variant at the location will be prohibited (suppressed) when the criterion is satisfied. The volume fraction of such a suppression field depends on temperature, defect concentration, and defect strength, as shown in **Figure 9*b***. The volume fraction of the suppression field for 3D percolation is approximately 0.68, which has predicted well the critical defect concentrations and glass transition temperatures in strain glass systems doped with different point defects (23).

4. CHALLENGES AND OUTLOOK

4.1. Unsolved Problems

As a newly discovered disordered state in ferroelastic systems, strain glass still prompts many unanswered questions. For example, suppression of autocatalysis by defects has been identified as the key to converting a normal martensitic transformation into a strain glass transition. However,

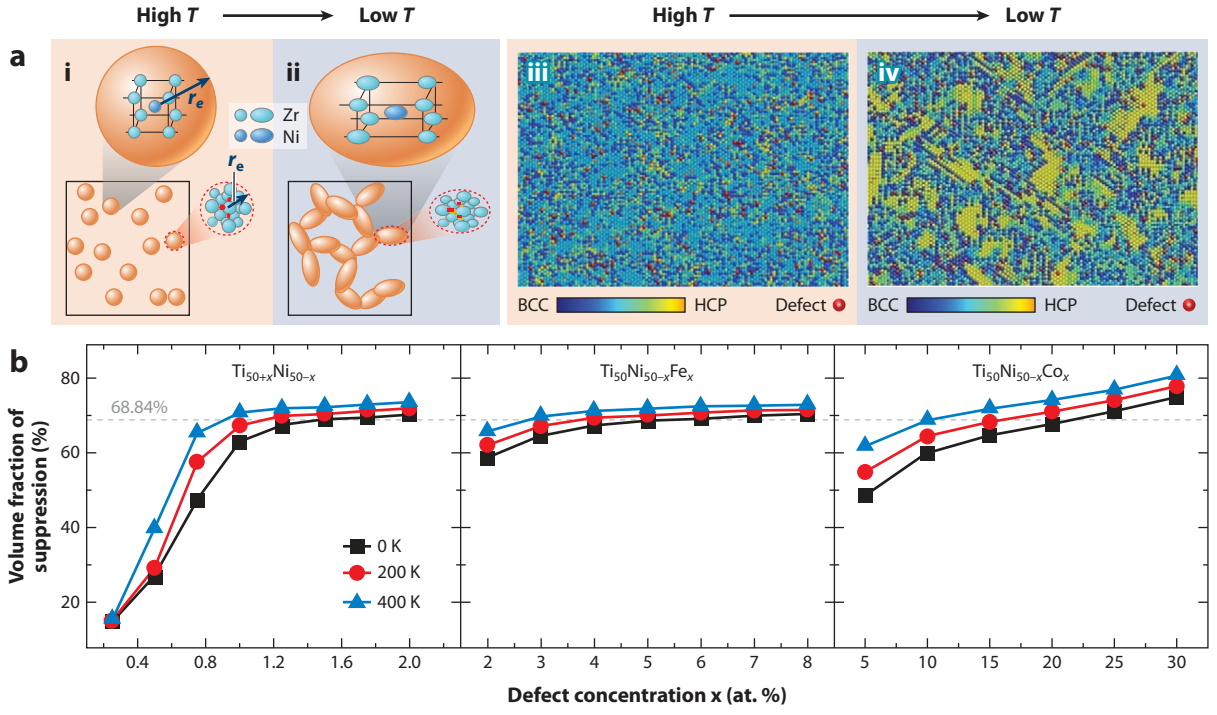

Figure 9

(*a*, *i* and *ii*) The formation of a strain network upon cooling. The point defects induce the strain cluster, and the strain clusters grow and form a percolated strain network. The orange circles represent the strain cluster caused by doped defects; the red, orange, and blue colors inside of the dashed circles represent the central effective dopant and other cluster atoms at high and low temperatures; r_e represents the radius of the strain cluster caused by defect. (*a*, *iii* and *iv*) Results of molecular dynamics simulations of ZrNi with atomic structures of strain glass with martensitic phase (*yellow*), parent phase (*blue*), and dopant atoms (*red*). (*b*) The required point defect concentrations for the percolation of a suppression field (that prevents the formation of given martensitic variants) at different temperatures, which is given by the intersections between the solid and dashed lines. Abbreviations: BCC, body-centered cubic; HCP, hexagonal close packed. Panel *a* adapted with permission from Reference 24; copyright 2020 American Physical Society. Panel *b* adapted with permission from Reference 23; copyright 2020 Elsevier.

direct ab initio and MD simulations of a strain glass transition are still lacking. Is the percolation threshold of a suppression field a good predictor of strain glass transition? In experiments, nanodomains of individual variants are observed in different strain glass systems, while in computer simulations, nanodomains of twinning martensite are also shown to have the unique properties of a strain glass transition. Are single-variant nanodomains of martensite necessary to define a strain glass state? The B19′ strain glass has shown a nearly linear SE with high strength (1.2 GPa), large recoverable strain (4%), and low elastic modulus (approximately 30 GPa) (30). Are these the optimal properties that one could achieve? What is the limit of the recoverable strain of a strain glass transition for a given stress-free transformation strain of the martensitic transformation? What is the lower limit of the apparent elastic modulus that could be achieved by a strain glass transition? Since strain glasses have nearly linear SE with slim hysteresis and high strength, excellent dimensional stability and functional fatigue resistance during stress or temperature cycling are expected. But both experimental and simulation studies are still lacking. Finally, the β relaxation is a general phenomenon in polymer and metallic glasses (125, 126), but there is no report of such a relaxation in strain glasses or ferroic glasses.

4.2. Future Work

The unique properties of strain glass transition are not surprising because it is similar to other nanostructured materials such as nanocrystalline materials (127), nanoscale multilayers (128), nanoprecipitates (129), nanoferromagnetic domains (130), nanopolarization domains (131), and nanocomposites (132), which are supposed to have unique properties compared to their microscale domain counterparts (133). Nanoscale martensitic domain engineering is the key to creating strain glass states and strain glass transitions. When each of the nanodomains can grow and produce local strains, a huge population of them will produce a large overall strain output. However, the random selection of variants by random fields associated with random defects will offer a limited amount of strain release. Thus, selection of only preferred variants by specially engineered defects or structural heterogeneities (such as deformation twins) for maximum strain output by strain glasses is highly desired. In situ TEM observations of stabilized martensitic domains by defects and the growth of these domains under applied load or upon cooling are also highly desired.

The insights gained by studying strain glass transition are beneficial to the design and optimization of other transforming materials (i.e., to use phase transformation to tailor materials properties), such as conventional SMAs (14, 134–137), transformation-induced plasticity/twinning-induced plasticity steels (138–140), and transformation-induced plasticity/twinning-induced plasticity Ti-alloys (141–143). In particular, concentration modulation–induced phase stability engineering (58), additive manufacturing (144, 145), accumulative roll bonding (146), multilayer deposition, and other new processing techniques could be used to tailor the structural phase transformations for controlled strain release and thus desired properties.

5. CONCLUSIONS

Strain glass is a new strain state in ferroelastic materials characterized by nanodomains of martensite. These nanodomains are created and confined by heterogeneous stress field and/or composition field at the nanoscale associated with random defects, including (but not limited to) point defects, dislocations, deformation twins, and precipitates, or by nanoscale concentration modulations produced by (but not limited to) spinodal decomposition, precipitation reaction, and multilayer deposition. When such heterogeneous fields percolate, they completely suppress autocatalysis and self-accommodation among different martensitic variants, as these fields are incompatible with long-range ordered, self-accommodating transformation strain domain patterns generated by normal martensitic transformations. As a consequence, the nanodomains of martensite cannot evolve into microscale twinning martensite such as the herringbone structure (i.e., a strain crystal state in normal martensite) upon cooling and are frozen into a strain glass state. Such a strain glass state has a few fundamental characteristics: its average structure is the same as that of the parent phase, it shows frequency dispersion in the storage modulus or internal friction, and it exhibits continuous splitting of zero-field-cooling and field-cooling curves.

The characteristics of a strain glass transition and all the unique properties associated with it are determined by how the nanodomains respond to an external field, either stress or temperature. Because the random defects have a broad distribution of potency to trigger locally martensitic transformation, the martensitic transformation starts and finishes at much higher temperatures or lower stresses in some local regions and at much lower temperatures or much higher stresses in other local regions. Because of the confinement from neighboring regions that are nonaccommodating, the growth of the nanodomains is limited for a given amount of undercooling or increment of the applied load. Collectively, these effects lead to an overall continuous transformation, with the disappearance of heat flow in DSC measurements, continuous electrical resistivity change, and continuous elastic modulus softening. Because strain glass transition is diffusionless, its response

to the external field is instantaneous. Thus, such a continuous transformation offers many unique properties, including nearly linear SE with large recoverable strain and slim hysteresis, ultralow elastic modulus with a broad temperature range, and Invar and Elinvar anomalies.

The key to creating a strain glass state is to engineer nanodomain structures of transformation strains (i.e., martensitic variants) by introducing internal random fields, either chemical or mechanical, with spatial variations at the nanometer scale. Point defect doping is an effective way to create strain glasses with relatively small transformation strains (a few present), such as the R phase. For martensitic systems with large transformation strains (approximately 10%), such as the B19 and B19′ phase, extended defects carrying much larger lattice distortions such as dislocations are required. For ferroelastic systems whose martensitic transformation temperature or stress is a strong function of alloy composition, creating nanoscale concentration modulations could be an effective way to engineer strain glasses as well.

The strain glass state and strain glass transition extend the theory of martensitic transformations, and a complete phase diagram of martensitic transformation plus strain glass transition in a ferroelastic system provides a blueprint in engineering strain domain microstructures by defect engineering for desired strain release.

DISCLOSURE STATEMENT

The authors are not aware of any affiliations, memberships, funding, or financial holdings that might be perceived as affecting the objectivity of this review.

ACKNOWLEDGMENTS

The authors would like to acknowledge fruitful discussions with Prof. Dipankar Banerjee. Y.W. would like to acknowledge support from the US National Science Foundation (grant number DMR-1923929). D.W. would like to acknowledge support from the National Natural Science Foundation of China (51931004 and 52171012). Y.J. would also like to acknowledge support from the National Natural Science Foundation of China (51701150, 51831006, and 52071257) and 111 Project 2.0 (BP2018008). X.R. would like to acknowledge support from a Japan Society for the Promotion of Science Kakenhi grant.

LITERATURE CITED

1. Otsuka K, Wayman CM, Nakai K, Sakamoto H, Shimizu K. 1976. Superelasticity effects and stress-induced martensitic transformations in Cu-Al-Ni alloys. *Acta Metall.* 24:207–26
2. Miyazaki S, Ohmi Y, Otsuka K, Suzuki Y. 1982. Characteristics of deformation and transformation pseudoelasticity in Ti-Ni alloys. *J. Phys.* 43:255–60
3. Perkins J, ed. 1975. *Shape Memory Effects in Alloys: Proceedings of the International Symposium on Shape Memory Effects and Applications Held in Toronto, Ontario, Canada, May 19–22, 1975*. New York: Plenum
4. Bhattacharya K. 2003. *Microstructure of Martensite: Why It Forms and How It Gives Rise to the Shape-Memory Effect*. Oxford/New York: Oxford Univ. Press
5. Cui J, Ren X. 2014. Elinvar effect in Co-doped TiNi strain glass alloys. *Appl. Phys. Lett.* 105:061904
6. Wang Y, Gao J, Wu H, Yang S, Ding X, et al. 2014. Strain glass transition in a multifunctional β-type Ti alloy. *Sci. Rep.* 4:3995
7. Qin F, Xiao W, Lu F, Ji Y, Zhao X, Ren X. 2019. Resolution of a discrepancy of magnetic mechanism for Elinvar anomaly in Fe-Ni based alloys. *J. Mater. Sci. Technol.* 35:396–401
8. Damjanovic D. 2005. Contributions to the piezoelectric effect in ferroelectric single crystals and ceramics. *J. Am. Ceram. Soc.* 88:2663–76
9. James RD, Wuttig M. 1998. Magnetostriction of martensite. *Philos. Mag. A* 77:1273–99

10. Li F, Jin L, Xu Z, Zhang SJ. 2014. Electrostrictive effect in ferroelectrics: an alternative approach to improve piezoelectricity. *Appl. Phys. Rev.* 1:011103
11. Fischer FD, Reisner G, Werner E, Tanaka K, Cailletaud G, Antretter T. 2000. A new view on transformation induced plasticity (TRIP). *Int. J. Plast.* 16:723–48
12. Soleimani M, Kalhor A, Mirzadeh H. 2020. Transformation-induced plasticity (TRIP) in advanced steels: a review. *Mater. Sci. Eng. A* 795:140023
13. Sun F, Zhang JY, Marteleur M, Gloriant T, Vermaut P, et al. 2013. Investigation of early stage deformation mechanisms in a metastable β titanium alloy showing combined twinning-induced plasticity and transformation-induced plasticity effects. *Acta Mater.* 61:6406–17
14. Otsuka K, Ren X. 2005. Physical metallurgy of Ti-Ni-based shape memory alloys. *Prog. Mater. Sci.* 50:511–678
15. Hartl DJ, Lagoudas DC. 2007. Aerospace applications of shape memory alloys. *Proc. Inst. Mech. Eng. Part G: J. Aerosp. Eng.* 221:535–52
16. Sreekumar M, Nagarajan T, Singaperumal M, Zoppi M, Molfino R. 2007. Critical review of current trends in shape memory alloy actuators for intelligent robots. *Ind. Robot* 34:285–94
17. Langbein S, Czechowicz A. 2012. Problems and solutions for shape memory actuators in automotive applications. In *Proceedings of the ASME 2012 Conference on Smart Materials, Adaptive Structures and Intelligent Systems*, Vol. 2: *Mechanics and Behavior of Active Materials; Integrated System Design and Implementation; Bio-Inspired Materials and Systems; Energy Harvesting*, pp. 433–39. Stone Mountain, GA: ASME
18. Sarkar S, Ren X, Otsuka K. 2005. Evidence for strain glass in the ferroelastic-martensitic system $Ti_{50-x}Ni_{50+x}$. *Phys. Rev. Lett.* 95:205702
19. Ren X, Wang Y, Zhou Y, Zhang Z, Wang D, et al. 2010. Strain glass in ferroelastic systems: premartensitic tweed versus strain glass. *Philos. Mag.* 90:141–57
20. Sherrington D. 2014. A spin glass perspective on ferroic glasses. *Phys. Status Solidi B* 251:1967–81
21. Ji YC, Wang D, Wang Y, Zhou YM, Xue DZ, et al. 2017. Ferroic glasses. *NPJ Comput. Mater.* 3:43
22. Semenovskaya S, Khachaturyan AG. 1992. Structural transformations in nonstoichiometric $YBa_2Cu_3O_{6+\delta}$. *Phys. Rev. B* 46:6511–34
23. Liang C, Wang D, Wang Z, Ding X, Wang Y. 2020. Revealing the atomistic mechanisms of strain glass transition in ferroelastics. *Acta Mater.* 194:134–43
24. Zong H, Wu H, Tao X, Xue D, Sun J, et al. 2019. Percolated strain networks and universal scaling properties of strain glasses. *Phys. Rev. Lett.* 123:015701
25. Wang D, Zhang Z, Zhang J, Zhou Y, Wang Y, et al. 2010. Strain glass in Fe-doped Ti–Ni. *Acta Mater.* 58:6206–15
26. Zhou Y, Xue D, Ding X, Wang Y, Zhang J, et al. 2010. Strain glass in doped $Ti_{50}(Ni_{50-x}D_x)$ (D = Co, Cr, Mn) alloys: implication for the generality of strain glass in defect-containing ferroelastic systems. *Acta Mater.* 58:5433–42
27. Ji Y, Ding X, Lookman T, Otsuka K, Ren X. 2013. Heterogeneities and strain glass behavior: role of nanoscale precipitates in low-temperature-aged $Ti_{48.7}Ni_{51.3}$ alloys. *Phys. Rev. B* 87:104110
28. Zhou Z, Cui J, Ren X. 2015. Strain glass state as the boundary of two phase transitions. *Sci. Rep.* 5:13377
29. Zhang J, Xue D, Cai X, Ding X, Ren X, Sun J. 2016. Dislocation induced strain glass in $Ti_{50}Ni_{45}Fe_5$ alloy. *Acta Mater.* 120:130–37
30. Liang Q, Wang D, Zhang J, Ji Y, Ding X, et al. 2017. Novel B19′ strain glass with large recoverable strain. *Phys. Rev. Mater.* 1:033608
31. Ji Y, Wang D, Ding X, Otsuka K, Ren X. 2015. Origin of an isothermal *R*-martensite formation in Ni-rich Ti-Ni solid solution: crystallization of strain glass. *Phys. Rev. Lett.* 114:055701
32. Ji YC, Ding XD, Wang D, Otsuka K, Ren XB. 2015. Glass-ferroic composite caused by the crystallization of ferroic glass. *Phys. Rev. B* 92:241114
33. Zhang JY, Mao YW, Wang D, Li J, Wang YZ. 2016. Accelerating ferroic ageing dynamics upon cooling. *NPG Asia Mater.* 8:e319
34. Zhang Z, Wang Y, Wang D, Zhou Y, Otsuka K, Ren X. 2010. Phase diagram of $Ti_{50-x}Ni_{50+x}$: crossover from martensite to strain glass. *Phys. Rev. B* 81:224102
35. Hao Y, Ji Y, Zhang Z, Yin M, Liu C, et al. 2019. Strain glass in $Ti_{50-x}Ni_{35+x}Cu_{15}$ shape memory alloys. *Scripta Mater.* 168:71–75

36. Zhou Y, Xue D, Ding X, Otsuka K, Sun J, Ren X. 2014. High temperature strain glass transition in defect doped Ti–Pd martensitic alloys. *Phys. Status Solidi B* 251:2027–33
37. Zhou Y, Xue D, Tian Y, Ding X, Guo S, et al. 2014. Direct evidence for local symmetry breaking during a strain glass transition. *Phys. Rev. Lett.* 112:025701
38. Ren S, Liu C, Chen X, Hao Y, Ren X. 2020. Strain glass by aging in Ti–Pd–Fe shape memory alloys. *Scripta Mater.* 177:11–16
39. Ren S, Liu C, Wang WH. 2021. High temperature strain glass in Ti-Au and Ti-Pt based shape memory alloys. *Chin. Phys. B* 30:018101
40. Sun X, Cong D, Ren Y, Liss K-D, Brown DE, et al. 2020. Magnetic-field-induced strain-glass-to-martensite transition in a Fe-Mn-Ga alloy. *Acta Mater.* 183:11–23
41. Wang DP, Chen X, Nie ZH, Li N, Wang ZL, et al. 2012. Transition in superelasticity for $Ni_{55-x}Co_xFe_{18}Ga_{27}$ alloys due to strain glass transition. *Europhys. Lett.* 98:46004
42. Nevgi R, Priolkar KR, Acet M. 2021. Strain glass versus antisite disorder induced ferromagnetic state in Fe doped Ni-Mn-In Heusler martensites. *J. Phys. D. Appl. Phys.* 54:185002
43. Wang Y, Huang C, Gao J, Yang S, Ding X, et al. 2012. Evidence for ferromagnetic strain glass in Ni-Co-Mn-Ga Heusler alloy system. 101:101913
44. Yao YG, Yang YD, Ren S, Zhou C, Li LL, Ren XB. 2012. Ferroelastic and strain glass transition in $(1-x)(Bi_{0.5}Na_{0.5})TiO_3$-$xBaTiO_3$ solid solution. *Europhys. Lett.* 100:17004
45. Ren S, Xue D, Ji Y, Liu X, Yang S, Ren X. 2017. Low-field-triggered large magnetostriction in iron-palladium strain glass alloys. *Phys. Rev. Lett.* 119:125701
46. Liu J, Jin M, Ni C, Shen Y, Fan G, et al. 2011. Strain glassy behavior and premartensitic transition in $Au_7Cu_5Al_4$ alloy. *Phys. Rev. B* 84:140102
47. Lloveras P, Castán T, Porta M, Planes A, Saxena A. 2008. Influence of elastic anisotropy on structural nanoscale textures. *Phys. Rev. Lett.* 100:165707
48. Lloveras P, Castán T, Porta M, Planes A, Saxena A. 2009. Glassy behavior in martensites: interplay between elastic anisotropy and disorder in zero-field-cooling/field-cooling simulation experiments. *Phys. Rev. B* 80:054107
49. Wang D, Lv D, Gao Y, Wang Y, Ren X, Wang Y. 2016. Defect strength and strain glass state in ferroelastic systems. *J. Alloy Compd.* 661:100–9
50. Ahadi A, Sun Q. 2014. Effects of grain size on the rate-dependent thermomechanical responses of nanostructured superelastic NiTi. *Acta Mater.* 76:186–97
51. Tadaki T, Wayman CM. 1980. Crystal-structure and microstructure of a cold-worked TiNi alloy with unusual elastic behavior. *Scr. Metall.* 14:911–14
52. Rathod CR, Clausen B, Bourke MAM, Vaidyanathan R. 2006. Neutron diffraction investigation of hysteresis reduction and increase in linearity in the stress-strain response of superelastic NiTi. *Appl. Phys. Lett.* 88:201919
53. Zheng YF, Huang BM, Zhang JX, Zhao LC. 2000. The microstructure and linear superelasticity of cold-drawn TiNi alloy. *Mater. Sci. Eng. A* 279:25–35
54. Tang Z, Wang Y, Liao X, Wang D, Yang S, Song X. 2015. Stress dependent transforming behaviors and associated functional properties of a nano-precipitates induced strain glass alloy. *J. Alloy Compd.* 622:622–27
55. Yu T, Gao Y, Casalena L, Anderson P, Mills M, Wang Y. 2021. H-phase precipitation and its effects on martensitic transformation in NiTi-Hf high-temperature shape memory alloys. *Acta Mater.* 208:116651
56. Zhu J, Wu H-H, Wu Y, Wang H, Zhang T, et al. 2021. Influence of Ni_4Ti_3 precipitation on martensitic transformations in NiTi shape memory alloy: R phase transformation. *Acta Mater.* 207:116665
57. Liu J-P, Wang Y-D, Hao Y-L, Wang Y, Nie Z-H, et al. 2013. New intrinsic mechanism on gum-like superelasticity of multifunctional alloys. *Sci. Rep.* 3:2156
58. Zhu J, Gao Y, Wang D, Zhang T-Y, Wang Y. 2017. Taming martensitic transformation via concentration modulation at nanoscale. *Acta Mater.* 130:196–207
59. Liang Q, Wang D, Zheng Y, Zhao S, Gao Y, et al. 2020. Shuffle-nanodomain regulated strain glass transition in Ti-24Nb-4Zr-8Sn alloy. *Acta Mater.* 186:415–24
60. Hao SJ, Cui LS, Jiang DQ, Han XD, Ren Y, et al. 2013. A transforming metal nanocomposite with large elastic strain, low modulus, and high strength. *Science* 339:1191–94

61. Wang D, Liang Q, Zhao S, Zhao P, Zhang T, et al. 2019. Phase field simulation of martensitic transformation in pre-strained nanocomposite shape memory alloys. *Acta Mater.* 164:99–109
62. Shapiro SM, Noda Y, Fujii Y, Yamada Y. 1984. X-ray investigation of the premartensitic phase in $Ni_{46.8}Ti_{50}Fe_{3.2}$. *Phys. Rev. B* 30:4314–21
63. Shindo D, Murakami Y, Ohba T. 2002. Understanding precursor phenomena for the R-phase transformation in Ti-Ni-based alloys. *MRS Bull.* 27:121–27
64. Otsuka K, Wayman CM. 1999. *Shape Memory Materials*. Cambridge, UK: Cambridge Univ. Press
65. Choi MS, Fukuda T, Kakeshita T, Mori H. 2006. Incommensurate–commensurate transition and nanoscale domain-like structure in iron doped Ti–Ni shape memory alloys. *Philos. Mag.* 86:67–78
66. Choi M-S, Fukuda T, Kakeshita T. 2005. Anomalies in resistivity, magnetic susceptibility and specific heat in iron-doped Ti–Ni shape memory alloys. *Scripta Mater.* 53:869–73
67. Wang Y, Ren XB, Otsuka K. 2008. Strain glass: glassy martensite. *Mater. Sci. Forum* 583:67–84
68. Wang D, Wang Y, Zhang Z, Ren X. 2010. Modeling abnormal strain states in ferroelastic systems: the role of point defects. *Phys. Rev. Lett.* 105:205702
69. Wang D, Hou S, Wang Y, Ding XD, Ren S, et al. 2014. Superelasticity of slim hysteresis over a wide temperature range by nanodomains of martensite. *Acta Mater.* 66:349–59
70. Zhang J, Wang Y, Ding X, Zhang Z, Zhou Y, et al. 2011. Spontaneous strain glass to martensite transition in a $Ti_{50}Ni_{44.5}Fe_{5.5}$ strain glass. *Phys. Rev. B* 84:214201
71. Hou S, Wang Y, Zhang J, Wang D, Ren S, Ren X. 2012. Evidence for crossover martensite in $Ti_{50}Ni_{45}Fe_5$: an intermediate state between normal martensite and strain glass. *Europhys. Lett.* 100:58001
72. Chien C, Tsao C-S, Wu S-K, Chang C-Y, Chang P-C, Kuo Y-K. 2016. Characteristics of the strain glass transition in as-quenched and 250°C early-aged $Ti_{48.7}Ni_{51.3}$ shape memory alloy. *Acta Mater.* 120:159–67
73. Wang Y, Zhou Y, Zhang J, Ding X, Yang S, et al. 2010. Evolution of the relaxation spectrum during the strain glass transition of $Ti_{48.5}Ni_{51.5}$ alloy. *Acta Mater.* 58:4723–29
74. Narayanaswamy OS. 1971. A model of structural relaxation in glass. *J. Am. Ceram. Soc.* 54:491–98
75. Bennemann C, Paul W, Binder K, Dünweg B. 1998. Molecular-dynamics simulations of the thermal glass transition in polymer melts: α-relaxation behavior. *Phys. Rev. E* 57:843–51
76. Slipenyuk A, Eckert J. 2004. Correlation between enthalpy change and free volume reduction during structural relaxation of $Zr_{55}Cu_{30}Al_{10}Ni_5$ metallic glass. *Scripta Mater.* 50:39–44
77. Wang Y, Ren X, Otsuka K, Saxena A. 2008. Temperature–stress phase diagram of strain glass $Ti_{48.5}Ni_{51.5}$. *Acta Mater.* 56:2885–96
78. Mydosh JA. 1993. *Spin Glasses: An Experimental Introduction*. London/Washington, DC: Taylor Francis
79. Ghosh G, Olson GB. 1994. Kinetics of F.C.C. → B.C.C. heterogeneous martensitic nucleation—I. The critical driving force for athermal nucleation. *Acta Metall. Mater.* 42:3361–70
80. Wang Y, Huang C, Wu H, Gao J, Yang S, et al. 2013. Spontaneous strain glass to martensite transition in ferromagnetic Ni-Co-Mn-Ga strain glass. *Appl. Phys. Lett.* 102:141909
81. Chu F, Setter N, Tagantsev AK. 1993. The spontaneous relaxor-ferroelectric transition of $Pb(Sc_{0.5}Ta_{0.5})O_3$. *J. Appl. Phys.* 74:5129–34
82. Chu F, Reaney IM, Setter N. 1995. Spontaneous (zero-field) relaxor-to-ferroelectric-phase transition in disordered $Pb(Sc_{1/2}Nb_{1/2})O_3$. *J. Appl. Phys.* 77:1671–76
83. Fang M, Ji Y, Zhang Z, Yang Y, Liu C, et al. 2018. Re-entrant relaxor–ferroelectric composite showing exceptional electromechanical properties. *NPG Asia Mater.* 10:1029–36
84. Wang Y, Ren X, Otsuka K, Saxena A. 2007. Evidence for broken ergodicity in strain glass. *Phys. Rev. B* 76:132201
85. Novák V, Šittner P, Dayananda GN, Braz-Fernandes FM, Mahesh KK. 2008. Electric resistance variation of NiTi shape memory alloy wires in thermomechanical tests: experiments and simulation. *Mater. Sci. Eng. A* 481–482:127–33
86. Ling HC, Kaplow R. 1980. Phase-transitions and shape memory in NiTi. *Metall. Trans. A* 11:77–83
87. Bag P, Chang P-C, Kuo Y-K, Wu S-K, Lin C, Li B-Y. 2019. Coexistence of martensite and strain glass phases in homogenized Ni-rich TiNi shape memory alloys. *Intermetallics* 109:16–23
88. Kartha S, Krumhansl JA, Sethna JP, Wickham LK. 1995. Disorder-driven pretransitional tweed pattern in martensitic transformations. *Phys. Rev. B* 52:803–22

89. Zhang LX, Wang D, Ren XB, Wang YZ. 2015. A new mechanism for low and temperature-independent elastic modulus. *Sci. Rep.* 5:11477
90. Zhou Y, Yuan R, Xue D, Wang D, Ding X, et al. 2021. Tailoring thermal expansion coefficient from positive through zero to negative in the compositional crossover alloy $Ti_{50}(Pd_{40}Cr_{10})$ by uniaxial tensile stress. *Mater. Des.* 199:109431
91. Demakov SL, Stepanov SI, Illarionov AG, Ryzhkov MA. 2017. Thermal-expansion anisotropy of orthorhombic martensite in the two-phase ($\alpha + \beta$) titanium alloy. *Phys. Met Metallogr.* 118:264–71
92. Khan PY, Ren S, Ma T, Ren X. 2020. Magnetostriction enhancement in ferromagnetic strain glass by approaching the crossover of martensite. *Appl. Phys. Lett.* 116:072402
93. Wang Y, Ren X, Otsuka K. 2006. Shape memory effect and superelasticity in a strain glass alloy. *Phys. Rev. Lett.* 97:225703
94. Semenovskaya S, Khachaturyan AG. 1997. Coherent structural transformations in random crystalline systems. *Acta Mater.* 45:4367–84
95. Levaniuk AP, Sigov AS. 1988. *Defects and Structural Phase Transitions*. New York: Gordon Breach Sci.
96. Vasseur R, Lookman T. 2010. Effects of disorder in ferroelastics: a spin model for strain glass. *Phys. Rev. B* 81:094107
97. Wang Y, Li J. 2010. Phase field modeling of defects and deformation. *Acta Mater.* 58:1212–35
98. Wang Y, Khachaturyan AG. 1997. Three-dimensional field model and computer modeling of martensitic transformations. *Acta Mater.* 45:759–73
99. Vasseur R, Xue D, Zhou Y, Ettoumi W, Ding X, et al. 2012. Phase diagram of ferroelastic systems in the presence of disorder: analytical model and experimental verification. *Phys. Rev. B* 86:184103
100. Salje EKH, Ding X, Aktas O. 2014. Domain glass. *Phys. Status Solidi B* 251:2061–66
101. Nguyen L, Wang D, Wang Y, De Graef M. 2015. Quantifying the abnormal strain state in ferroelastic materials: a moment invariant approach. *Acta Mater.* 94:172–80
102. Gao Y, Zhou N, Yang F, Cui Y, Kovarik L, et al. 2012. P-phase precipitation and its effect on martensitic transformation in (Ni,Pt)Ti shape memory alloys. *Acta Mater.* 60:1514–27
103. Zhou N, Shen C, Wagner MFX, Eggeler G, Mills MJ, Wang Y. 2010. Effect of Ni_4Ti_3 precipitation on martensitic transformation in Ti–Ni. *Acta Mater.* 58:6685–94
104. Zhang W, Jin YM, Khachaturyan AG. 2007. Modelling of dislocation-induced martensitic transformation in anisotropic crystals. *Philos. Mag.* 87:1545–63
105. Xu YC, Rao WF, Morris JW, Khachaturyan AG. 2018. Nanoembryonic thermoelastic equilibrium and enhanced properties of defected pretransitional materials. *NPJ Comput. Mater.* 4:58
106. Javanbakht M, Levitas VI. 2015. Interaction between phase transformations and dislocations at the nanoscale. Part 2: phase field simulation examples. *J. Mech. Phys. Solids* 82:164–85
107. Kundin J, Raabe D, Emmerich H. 2011. A phase-field model for incoherent martensitic transformations including plastic accommodation processes in the austenite. *J. Mech. Phys. Solids* 59:2082–102
108. Ren S, Zhou C, Xue DZ, Wang D, Zhang J, et al. 2016. Sandwichlike strain glass phase diagram of $Ti_{49}Ni_{51-x}Pd_x$. *Phys. Rev. B* 94:214112
109. Nii Y, Arima T, Kim HY, Miyazaki S. 2010. Effect of randomness on ferroelastic transitions: disorder-induced hysteresis loop rounding in Ti-Nb-O martensitic alloy. *Phys. Rev. B* 82:214104
110. Robertson IM, Wayman CM. 1983. Tweed microstructures I. Characterization in β-NiAl. *Philos. Mag. A* 48:421–42
111. Koike J, Parkin DM, Nastasi M. 1990. Crystal-to-amorphous transformation of NiTi induced by cold rolling. *J. Mater. Res.* 5:1414–18
112. Gall K, Tyber J, Wilkesanders G, Robertson SW, RO Ritchie, Maier HJ. 2008. Effect of microstructure on the fatigue of hot-rolled and cold-drawn NiTi shape memory alloys. *Mater. Sci. Eng. A* 486:389–403
113. Liang Q, Kloenne Z, Zheng Y, Wang D, Antonov S, et al. 2020. The role of nano-scaled structural non-uniformities on deformation twinning and stress-induced transformation in a cold rolled multifunctional β-titanium alloy. *Scripta Mater.* 177:181–85
114. Antonov S, Kloenne Z, Gao Y, Wang D, Feng Q, et al. 2020. Novel deformation twinning system in a cold rolled high-strength metastable-β Ti-5Al-5V-5Mo-3Cr-0.5Fe alloy. *Materialia* 9:100614
115. Gao Y. 2019. Symmetry and pathway analyses of the twinning modes in Ni–Ti shape memory alloys. *Materialia* 6:100320

116. McCormick PG, Liu Y. 1994. Thermodynamic analysis of the martensitic transformation in NiTi—II. Effect of transformation cycling. *Acta Metall. Mater.* 42:2407–13
117. Melton KN, Mercier O. 1979. Fatigue of NiTi thermoelastic martensites. *Acta Metall.* 27:137–44
118. Eggeler G, Hornbogen E, Yawny A, Heckmann A, Wagner M. 2004. Structural and functional fatigue of NiTi shape memory alloys. *Mater. Sci. Eng. A* 378:24–33
119. Guo W, Steinbach I, Somsen C, Eggeler G. 2011. On the effect of superimposed external stresses on the nucleation and growth of Ni_4Ti_3 particles: a parametric phase field study. *Acta Mater.* 59:3287–96
120. Khalil-Allafi J, Dlouhy A, Eggeler G. 2002. Ni_4Ti_3-precipitation during aging of NiTi shape memory alloys and its influence on martensitic phase transformations. *Acta Mater.* 50:4255–74
121. Khalil Allafi J, Ren X, Eggeler G. 2002. The mechanism of multistage martensitic transformations in aged Ni-rich NiTi shape memory alloys. *Acta Mater.* 50:793–803
122. Favier D, Liu Y, Orgéas L, Sandel A, Debove L, Comte-Gaz P. 2006. Influence of thermomechanical processing on the superelastic properties of a Ni-rich Nitinol shape memory alloy. *Mater. Sci. Eng. A* 429:130–36
123. Qin S-J, Shang J-X, Wang F-H, Chen Y. 2017. The role of strain glass state in the shape memory alloy $Ni_{50+x}Ti_{50-x}$: insight from an atomistic study. *Mater. Des.* 120:238–54
124. Stonaha PJ, Karaman I, Arroyave R, Salas D, Bruno NM, et al. 2018. Glassy phonon heralds a strain glass state in a shape memory alloy. *Phys. Rev. Lett.* 120:245701
125. Yu HB, Shen X, Wang Z, Gu L, Wang WH, Bai HY. 2012. Tensile plasticity in metallic glasses with pronounced β relaxations. *Phys. Rev. Lett.* 108:015504
126. Popli R, Glotin M, Mandelkern L, Benson RS. 1984. Dynamic mechanical studies of α and β relaxations of polyethylenes. *J. Polym. Sci.* 22:407–48
127. Gleiter H. 1991. *Nanocrystalline Materials*. Berlin/Heidelberg, Ger.: Springer
128. Hammond PT. 2004. Form and function in multilayer assembly: new applications at the nanoscale. *Adv. Mater.* 16:1271–93
129. Cheng S, Zhao YH, Zhu YT, Ma E. 2007. Optimizing the strength and ductility of fine structured 2024 Al alloy by nano-precipitation. *Acta Mater.* 55:5822–32
130. Niebieskikwiat D, Salamon MB. 2005. Intrinsic interface exchange coupling of ferromagnetic nanodomains in a charge ordered manganite. *Phys. Rev. B* 72:174422
131. Shvartsman VV, Kholkin AL, Orlova A, Kiselev D, Bogomolov AA, Sternberg A. 2005. Polar nanodomains and local ferroelectric phenomena in relaxor lead lanthanum zirconate titanate ceramics. *Appl. Phys. Lett.* 86:202907
132. Ajayan PM, Schadler LS, Braun PV. 2003. *Nanocomposite Science and Technology*. Weinheim, Ger.: Wiley-VCH
133. Moriarty P. 2001. Nanostructured materials. *Rep. Prog. Phys.* 64:297–381
134. Van Humbeeck J. 2001. Shape memory alloys: a material and a technology. *Adv. Eng. Mater.* 3:837–50
135. Eggeler G, Hornbogen E, Yawny A, Heckmann A, Wagner M. 2004. Structural and functional fatigue of NiTi shape memory alloys. *Mater. Sci. Eng. A* 378:24–33
136. Zhang J, Somsen C, Simon T, Ding X, Hou S, et al. 2012. Leaf-like dislocation substructures and the decrease of martensitic start temperatures: a new explanation for functional fatigue during thermally induced martensitic transformations in coarse-grained Ni-rich Ti–Ni shape memory alloys. *Acta Mater.* 60:1999–2006
137. Simon T, Kröger A, Somsen C, Dlouhy A, Eggeler G. 2010. On the multiplication of dislocations during martensitic transformations in NiTi shape memory alloys. *Acta Mater.* 58:1850–60
138. De Cooman BC, Estrin Y, Kim SK. 2018. Twinning-induced plasticity (TWIP) steels. *Acta Mater.* 142:283–362
139. De Cooman BC. 2004. Structure–properties relationship in TRIP steels containing carbide-free bainite. *Curr. Opin. Solid State Mater. Sci.* 8:285–303
140. Grässel O, Krüger L, Frommeyer G, Meyer LW. 2000. High strength Fe–Mn–(Al, Si) TRIP/TWIP steels development — properties — application. *Int. J. Plast.* 16:1391–409
141. Zhang J, Tasan CC, Lai MJ, Dippel AC, Raabe D. 2017. Complexion-mediated martensitic phase transformation in titanium. *Nat. Commun.* 8:14210

142. Zhao G-H, Xu X, Dye D, Rivera-Díaz-del-Castillo PEJ. 2020. Microstructural evolution and strain-hardening in TWIP Ti alloys. *Acta Mater.* 183:155–64
143. Marteleur M, Sun F, Gloriant T, Vermaut P, Jacques PJ, Prima F. 2012. On the design of new β-metastable titanium alloys with improved work hardening rate thanks to simultaneous TRIP and TWIP effects. *Scripta Mater.* 66:749–52
144. Hou HL, Simsek E, Ma T, Johnson NS, Qian SX, et al. 2019. Fatigue-resistant high-performance elastocaloric materials made by additive manufacturing. *Science* 366:1116
145. Zhang T, Huang Z, Yang T, Kong H, Luan J, et al. 2021. In situ design of advanced titanium alloy with concentration modulations by additive manufacturing. *Science* 374:478–82
146. Pirgazi H, Akbarzadeh A, Petrov R, Kestens L. 2008. Microstructure evolution and mechanical properties of AA1100 aluminum sheet processed by accumulative roll bonding. *Mater. Sci. Eng. A* 497:132–38

Annual Review of Materials Research

Volume 52, 2022

Contents